

# We are IntechOpen, the world's leading publisher of Open Access books Built by scientists, for scientists

6,900

Open access books available

185,000

International authors and editors

200M

Downloads

Our authors are among the

154

Countries delivered to

TOP 1%

most cited scientists

12.2%

Contributors from top 500 universities



WEB OF SCIENCE™

Selection of our books indexed in the Book Citation Index  
in Web of Science™ Core Collection (BKCI)

Interested in publishing with us?  
Contact [book.department@intechopen.com](mailto:book.department@intechopen.com)

Numbers displayed above are based on latest data collected.  
For more information visit [www.intechopen.com](http://www.intechopen.com)



## Bone: A Composite Natural Material

Maria Fátima Vaz<sup>1</sup>, Helena Canhão<sup>2</sup> and João Eurico Fonseca<sup>2</sup>

*<sup>1</sup>ICEMS and Mechanical Engineering Department,*

*Instituto Superior Técnico, Technical University of Lisbon,*

*<sup>2</sup>Rheumatology Research Unit, Instituto de Medicina Molecular, Faculty of Medicine,*

*University of Lisbon and Rheumatology Department, Santa Maria Hospital, Lisbon, Portugal*

### 1. Introduction

Composite materials are solids with two or more distinct constituents at a larger scale than an atomic one (Hull, 1981). In accordance to this definition, materials or biological tissues such as wood, dentin and bone are regarded as composite natural materials (Cowin, 2001; Lakes, 2003; Park & Lakes, 1992). Bone is regarded as a natural composite material, which appears as it is in nature, rather than the artificial or man made composites.

As for other composite materials, the mechanical properties of bone are dependent on its composition and structure, which includes the arrangement of the components and the bond between fibers and matrix. For example, the arrangement of fibers is different in several types of bones, gives rise to distinct properties.

An understanding of the mechanical behavior of bone is extremely important for the evaluation of fracture risk. Some types of bones, like vertebrae are constantly submitted to compressive loads and have an increased risk of fracture. Most bones are composed by outer cortical bone and an inner trabecular bone. Fractures on vertebrae, hip and wrist tend to start the global structural failing process in the regions of trabecular bone with decreased bone mass and microarchitecture changes (Fratzl & Weinkamer, 2007; Gibson & Ashby, 1999).

The emphasis of this chapter will be on the structure and mechanical properties of bone and how some diseases affect the material's characteristics. This chapter has two main sections. Firstly, we will describe the structure of bone at different scales, including the two different types of bone, cortical and trabecular. As growth and remodeling are key processes in the continuous renewal of bone, the issue will be also focused in this section. Several techniques can be used to characterize the hierarchical structure of bone. A particular emphasis will be given to transmission electron microscopy, scanning electron microscopy, second-harmonic generation imaging with a two-photon microscope, microcomputed tomography, quantitative backscattered electron imaging, atomic force microscopy, small angle X-ray scattering and neutron scattering.

The remaining part of the chapter will be devoted to the mechanical behavior of bone. As bones are often submitted to different types of external loadings, several types of tests will be reviewed namely compression, tension, bending, fatigue, creep, torsion and nanoindentation. Compression tests on femoral epiphysis of patients submitted to total hip

replacement surgery will also be discussed. Some aspects of the bone deformation mechanisms will also be approached.

Subsections will be devoted to the effect of a) metabolic bone diseases and b) inflammatory diseases on both structural and mechanical properties. Animal models are useful to reproduce human bone behavior on an experimental controlled environment and will be addressed. Besides the animal model, relevance will also be given in both subsections to human bone characterization. These issues will be discussed and illustrated using results from studies performed by the authors.

In summary, in this chapter, the authors will review the principal concepts of bone structure, microarchitecture and biomechanics in physiologic and pathologic states and will enrich this state of the art with a discussion of their own original results.

## 2. Structure

This section will be dedicated to the description of the structure of the bone at different scales, as well as, to the techniques used for structural characterization.

### 2.1 Structure at different scales

Bone has a complex hierarchical structure which will be analysed at different scales, in different subsections. In a continuous upsizing analysis we will address the molecular level (molecular structure of the constituents), the nanometer scale (fibril arrays of collagen and mineral phases), the submicrostructure scale (the intrinsic lamellae structure), the microstructural point of view (Haversian systems, osteons and trabeculae) and the macrostructural (cortical and trabecular bone).

#### 2.1.1 Structure from the molecular to the nanometer scale

Bone has a hierarchical ordered structure, and at a nanometer-scale can be compared to a composite material, composed by type I collagen fibers reinforced with calcium phosphate crystals (Fratzl et al., 2004; Park & Lakes, 1992). Water constitutes around 25% of the weight of fresh bone, essentially localized inside blood vessels in Haversian canals (Weiner & Wagner, 1998). The inorganic phase is composed essentially by carbonated apatite ( $\text{Ca}_5(\text{PO}_4, \text{CO}_3)_3(\text{OH})$ ), which presents as small crystals. In dry bone it accounts for almost two-thirds of bone weight. The remaining weight corresponds to organic material, which is essentially collagen, but there are also non-collagen proteins and lipids (Fratzl & Weinkamer, 2007).

Collagen is related to the capacity of bone to absorb energy, *i.e.* to the toughness, while the mineral phase plays an important role on the stiffness of the tissue (Viguet-Carrin et al., 2006).

Collagen is the most abundant protein in mammals and is formed by molecules that have a length around 280 to 300 nm and a diameter of 1.5 nm (Buehler, 2006; Fratzl et al., 2004; Fratzl & Weinkamer, 2007; Weiner & Wagner, 1998). The collagen molecule is composed by three polypeptide chains, which form a triple helix molecule (Figure 1a)) (Fratzl & Weinkamer, 2007; Weiner & Traub, 1992).

Collagen molecules are staggered, but there is a gap zone or spacing between them in the order of 35nm (Fratzl et al., 2004; Fratzl & Weinkamer, 2007; Weiner & Traub, 1992). Changes on the spacing, orientation, length of collagen molecules and the strength of intermolecular interactions, may give rise to different mechanical responses of the collagen

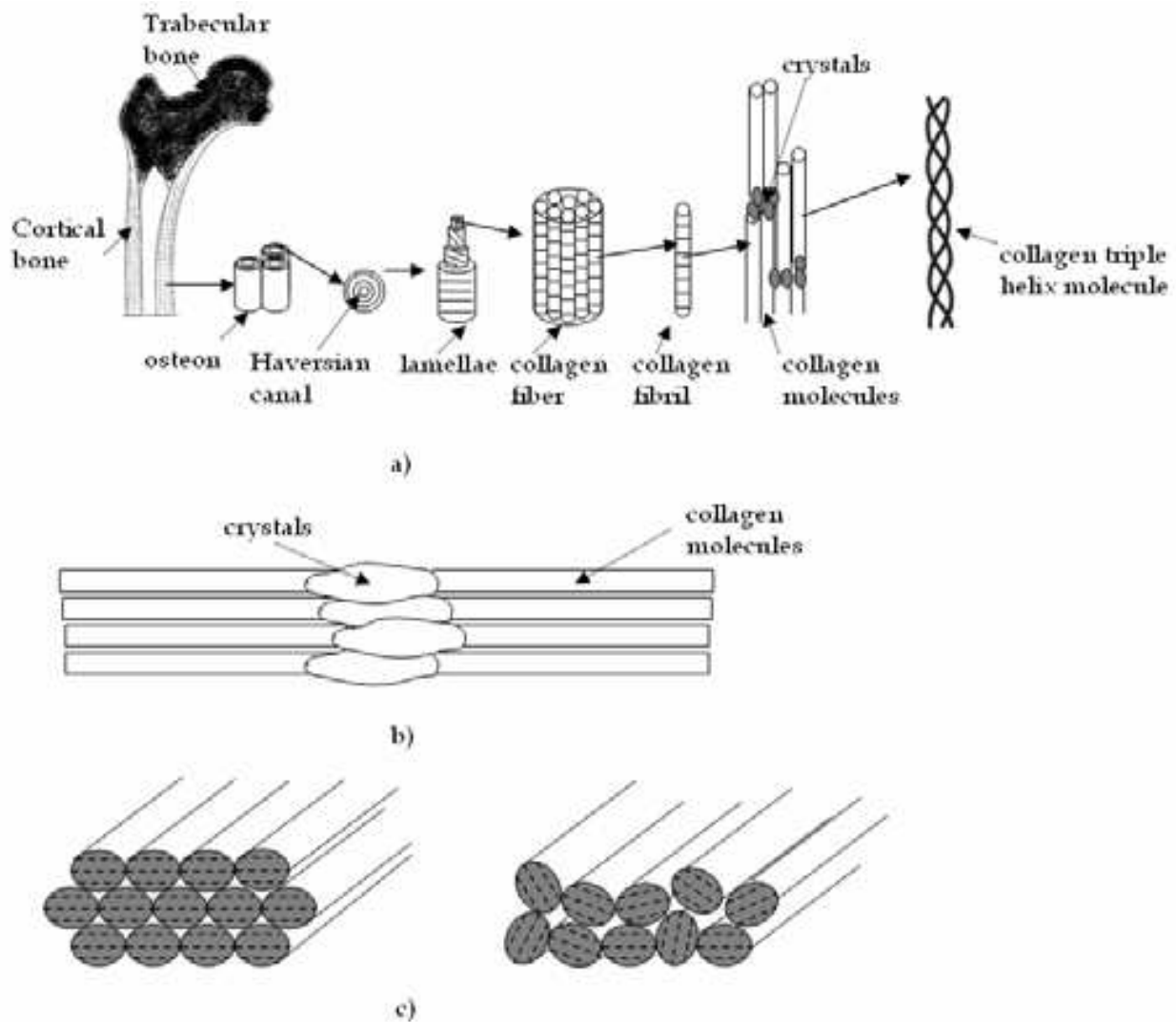


Fig. 1. a) Scheme of bone at different scale ranges (adapted from (Rho, et al., 1998)), b) arrangement of the apatite crystals which are aligned with the longitudinal direction of collagen fibers, c) inside one fiber, the fibrils may be aligned with respect to crystal axes and fibril axes, or the fibrils may have only an alignment of the fibril axes (adapted from (Weiner & Wagner 1998))

fibrils array (Buehler, 2006). The gaps between collagen molecules are sites for the nucleation of the calcium crystals (Fratzl & Weinkamer, 2007; Viguet-Carrin et al., 2006). Crystal size and orientation are influenced by collagen organization (Viguet-Carrin et al., 2006). However, the interface between collagen and apatite crystals is not well known (Weiner & Wagner, 1998). Mineral crystals of calcium phosphate particles deposit on the collagen array in the form of flat plates (Weiner & Traub, 1992). The crystals are essentially parallel to each other and to the axis of the collagen fibrils and occur at regular intervals along the fibrils at distances corresponding to the distances between collagen molecules (Figure 1b)). The arrangement of apatite crystals which are aligned with the longitudinal direction of collagen fibers is responsible for the anisotropic properties of bone, giving rise to higher values of stiffness and strength in that direction (Gibson & Ashby, 1999). The size, shape, arrangement and volume fraction of the crystals influence the mechanical behavior of bone (Fratzl et al., 2004). The distribution of crystals is not uniform in bone due to several

factors which involve bone remodeling, with zones with different degrees of mineralization, which are important in crack initiation and propagation (Fratzl et al., 2004). Mineral crystals have a plate shape with a wide range of dimensions. The thickness of the crystals is around 2-7 nm, while the length varies from 15 to 200 nm and the width from 10 to 80 nm (Fratzl et al., 2004; Fratzl & Weinkamer, 2007; Weiner & Traub, 1992; Weiner & Wagner, 1998). In the early stages of mineralization, crystal growth is limited by the collagen fibers, keeping the crystals separated. However, as growing progresses, crystals continue to grow and eventually join, which influences the mechanical properties of the fibrils (Giraud-Guille, 1988). In such conditions crystals maintain their plate-like shape but become very thin (Fratzl & Weinkamer, 2007). Finally collagen molecular arrangement, cross-linking and molecular packing are important factors for bone properties (Fratzl et al., 2004; Viguet-Carrin et al., 2006).

### 2.1.2 Structure from the submicrostructure to the microstructure scale

The molecules of mineralized collagen form fibrils by a self assembling process with dimensions of 0.5 to 1  $\mu\text{m}$  (Fratzl et al., 2004; Weiner & Wagner, 1998). A mineralized collagen fibril has a higher stiffness, strength and energy until failure comparing to a pure collagen fibril showing that mineralization is a crucial step for normal bone properties (Buehler, 2007).

Fibrils also assemble parallel to each other into fibers (circa 10  $\mu\text{m}$ ) (Buehler, 2006; Fratzl et al., 2004; Fratzl, & Weinkamer, 2007). Inside each fiber, fibrils may be aligned following both crystal axes and fibril axes, or on the contrary the fibrils may have only an alignment of the fibril axes, as can be seen in Figure 1c (Weiner & Wagner, 1998). In the first case, the structure will have orthotropic symmetry, while the other organization will exhibit transversal isotropy.

Fibers may arrange at a lamellar type or at a woven type. The mineralized collagen fibers can arrange in a defined configuration giving rise to lamellar bone, or may be disposed with no particular pattern, which originates woven bone (Rho et al., 1998). Woven bone is found at early stages of mineralization (Weiner & Wagner, 1998). Cortical bone can exist on the form of woven or lamellar, but is mostly lamellar.

As the name suggests, the lamellar bone is made of lamellae at a micrometer range (Fratzl et al., 2004; Fratzl, & Weinkamer, 2007; Rho et al., 1998; Weiner & Traub, 1992; Weiner & Wagner, 1998). Lamellae are planar arrangements (3-7  $\mu\text{m}$ ) formed by bundles of collagen fibers (Weiner & Traub, 1992). Lamellae, lacunae, canaliculi and cement lines are present in the bone at the same structural level. Lamellar arrangements can be found in plexiform or osteonal bones in the cortical aspect. Plexiform bone has the appearance of a brick structure, with the lamellae sandwiched between nonlamellar bone layers (Weiner & Wagner, 1998). Plexiform bone is rarely present in humans, but can be found in animals (Weiner & Wagner, 1998).

In osteonal cortical bone, the lamellae in the sheet form, wrap into concentric layers of 3 to 8 lamellae around a canal filled with a blood vessel, giving rise to an osteon (Rho et al., 1998). It is classic to distinguish between primary and secondary osteons (Weiner & Wagner, 1998). Primary osteons contain a less amount of lamellae and smaller vascular channels in comparison with secondary osteons. Secondary osteons appear due to the replacement of bone by remodeling. Haversian systems or secondary osteons have a cylindrical shape (diameter 200 to 250  $\mu\text{m}$ ) and run parallel to the long axis of bone (Rho et al., 1998; Weiner & Wagner, 1998).

Lamellae, around an osteon, can be classified according to the Ascenzi group (Boyde et al., 1984) into a orthogonal plywood organization with alternate lamellae containing fiber orientation parallel and perpendicular to the axis of the osteon or into a unidirectional plywood for which the fiber orientation on the lamellae is longitudinal or transverse to the osteon axis (Fratzl, & Weinkamer, 2007). The Giraud-Guille model (Giraud-Guille, 1988) suggests that there is a change in the orientation of fibers, inside each lamellae (Figure 2), with angles that can reach  $90^\circ$ . Experimental observations suggest that inside each lamella, there are layers of sublamella (Weiner et al., 1999). The collagen fibers within the same sublamellae are essentially parallel to each other, while the orientation of collagen fibers between adjacent sublamellae may change (Fratzl, & Weinkamer, 2007), as seen in Figure 2c).

According to this model, adjacent lamellae have different orientations as they can be arranged longitudinally to the collagen fibers that are parallel to the axis of the arrangement or transversal to the collagen fibers, which run perpendicularly to the long axis (Rho et al., 1998).

The trabecular bone has a different arrangement of the lamellae in comparison with cortical bone, which are organized longitudinally along the trabeculae instead of concentrically (Fratzl, & Weinkamer, 2007). However, the several layers of lamellae may have different mineral contents (Fratzl, & Weinkamer, 2007).

Osteocyte lacunae and canaliculi are holes present in bone, containing osteocytes. These mature cells evolved from the osteoblasts and were trapped during the mineralization process (Bonewald, 2011). The diameter of the lacunae is around 10 to 20  $\mu\text{m}$  (Bonewald, 2011). Canaliculi are channels that connect the lacunae and represent the entrapment of cytoplasmic extensions that interconnect osteocytes. Cement lines result from remodeling and have a thicknesses ranging from 1 to 5  $\mu\text{m}$  (Nicoletta et al., 2011).

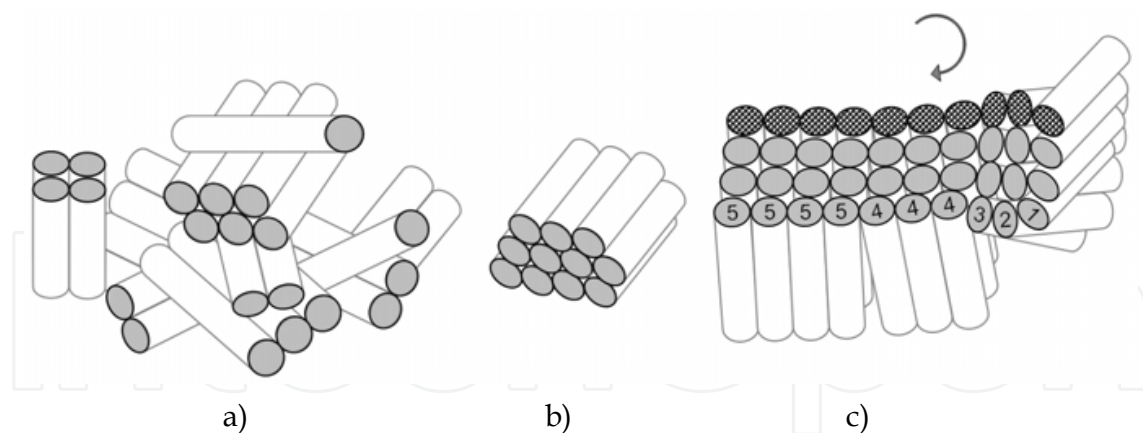


Fig. 2. Orientation of the fibers inside a lamellae: a) woven, b) parallel fibers (lamellar), c) plywood lamellar showing change in the orientation of fibers, inside one lamellae, with angles that can reach  $90^\circ$  (adapted from (Weiner & Wagner, 1998; Weiner et al., 1999))

### 2.1.3 Structure at microscopic level

The cortical bone structure is characterized by concentric layers around a blood vessel, which are denoted by osteons or Haversian systems. The Volkmann's canals are channels that connect transversely the blood vessels that are inside the Haversian canals (Fratzl, & Weinkamer, 2007).

The trabecular bone has a cellular structure made of an interconnected network of rods and plates forming an open cell foam (Gibson & Ashby, 1999; Gibson, 2005). The walls of the cell foam are limited by trabeculae which have a thickness around 200  $\mu\text{m}$  (Fratzl, & Weinkamer, 2007). Trabeculae are surrounded by bone marrow and living cells.

The trabeculae exhibit some osteocyte lacunae which connect to each other and to the exterior by the channels called canaliculi (Fratzl, & Weinkamer, 2007).

#### 2.1.4 Structure at a macrostructure scale

Taking a femur as an example of a long bone, at a macroscopic structural level, one can observe distinct parts with different characteristics, with trabecular (or cancellous or spongy) zones surrounded or protected by a cortical (or compact) shield (see Figure 3a)). Vertebra (Figure 3b) and c)), have also a shell of cortical bone that surrounds the trabecular area.

Trabecular bone has a porosity around 80% (Figure 3d)) while cortical bone is denser and has a porosity of less than 6% (Figure 3e)) (Fratzl & Weinkamer, 2007; Gibson & Ashby, 1999; Gibson, 2005).

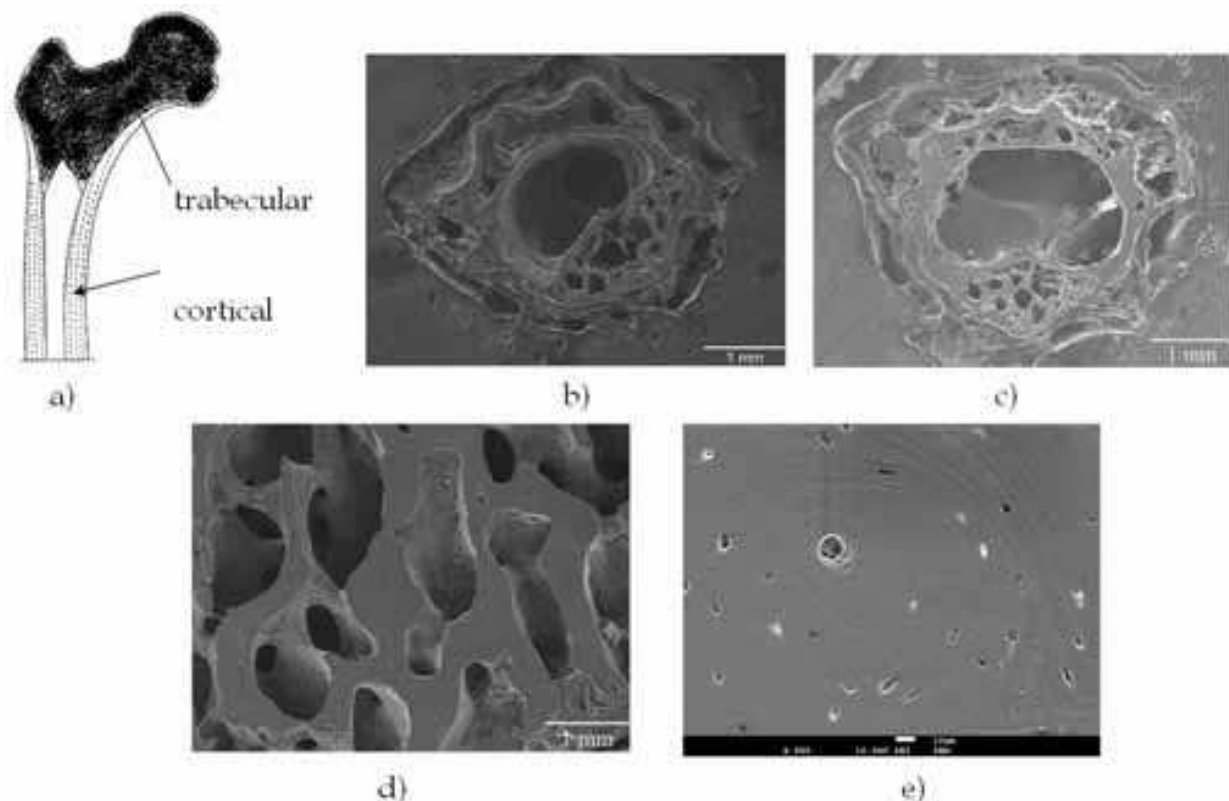


Fig. 3. a) Scheme of a femoral head with indication of trabecular and cortical zones. SEM pictures of: b) arthritic mouse vertebra, c) control mouse vertebra, d) human trabecular bone and e) of cortical equine bone

#### 2.2 Chemical composition and density

Compact bone and trabecular bone have almost the same elemental composition. Even arthritic bone, in an animal model, has a similar composition compared to control, with calcium=73% and phosphorus=27% (Caetano-Lopes et al., 2009a).

The density of the compact bone is in the range of 1800-2000 kg/m<sup>3</sup>, while the density of each trabeculae is 1820 kg/m<sup>3</sup>. The porosity however is much higher in trabecular bone, reaching 80%. As for other cellular materials, density of trabecular bone is usually calculated as the ratio between the density of bone and the density of a single trabeculae (Gibson & Ashby, 1999).

### **2.3 The effect of growth and remodeling on the structure of bone**

Natural materials, such as bone, have a growing process that is continually responding and adapting to environmental requirements. Bone is modified either by cellular activity during growth, as a response to systemic hormones, by the response to mechanical stress applied to the skeleton and by other environmental and genetic factors.

Bone is a dynamic structure under permanent remodeling. During childhood and adolescence, bone remodeling contributes to linear growth and to bone mass increase. Peak bone mass is attained around 25-30 years old. After this age bone starts slowly to change the metabolic activity, leading to progressive bone loss. The growth and remodeling process allow a renewal of the material. During bone remodeling, both osteoclast-mediated bone resorption of old material and osteoblast-mediated new bone matrix production occurs.

Cancellous bone is remodeled more often than the cortical bone (Rho et al., 1998).

As a consequence of bone remodeling, collagen fibers align along the direction of the load of the mature bone, which provides an increase in the mechanical strength (Caetano-Lopes et al., 2010).

### **2.4 Techniques for structure characterization**

Image techniques have attracted much interest lately and provide important insights on the characterization of bone structure. For example, the size and shape of mineral particles can be analyzed by transmission electron microscopy (Weiner & Traub, 1992). In this section, emphasis will be also given to scanning electron microscopy, second-harmonic generation imaging with a two-photon microscope, microcomputed tomography, quantitative backscattered electron imaging and atomic force microscopy. The techniques of small angle X-ray scattering and neutron scattering will be briefly mentioned.

#### **2.4.1 Transmission electron microscopy, TEM**

Transmission electron microscopy uses an electron beam that is transmitted through the specimen, generating an image by the interactions beam-sample. TEM requires extremely thin samples (Goodhew & Humphreys, 2000).

Transmission electron microscopy is used to image the nanostructure of bone, such as, collagen fibrils and apatite crystals and to analyze the size and shape of bone mineral particles (Fratzl et al., 2004; Rubin et al., 2004; Weiner & Traub, 1992; Weiner et al., 1999). TEM can be used in human (Fratzl et al., 2004; Weiner & Traub, 1992; Weiner et al., 1999) and in animal bone (Rubin et al., 2004; Weiner et al., 1999). Collagen organization can be studied by TEM, after the mineral removal (Weiner et al., 1999).

While the majority of studies describe mineral particles with a plate shape, some refer to needle shape (Fratzl et al., 2004). The dimensions of platelets range from 2 to 7nm in thickness, 15 to 200 nm in length and 10 to 80 nm of width (Fratzl et al., 2004).

#### **2.4.2 Scanning electron microscopy, SEM**

Scanning electron microscopy (SEM) uses an electron beam to scan the surface of a sample (Goodhew & Humphreys, 2000). Different interactions can be obtained when the electron

beam hits the material, including secondary electrons (SE), back-scattered electrons (BSE), characteristic X-ray and others (Goodhew & Humphreys, 2000). Secondary electrons have lower energy as they result from inelastic collisions between the incident beam and the sample, but produce very high resolution images with a large field depth. Back-scattered electrons consist of high energy electrons that are produced from elastic collisions among incident beam and material (Goodhew & Humphreys, 2000). BSE are used to detect contrast between regions with different chemical compositions as the intensity of the BSE signal depends on the atomic number of the specimen.

The preparation of bone samples to be observed in SEM is simple. If the bone sample is small, it does not need any previous procedure, but if it is large, a sample of dimensions of 1 cm of length must be obtained by cutting or drilling. After this procedure and completely defatted, the sample is mounted in resin, polished with grid papers and coated with a gold layer (Caetano-Lopes et al., 2009a, 2010).

SEM is a powerful tool to characterize the superficial structure of bone. SEM can be used at the macroscopic scale, from the submicrostructure to the microstructure scale, for example to observe the trabeculae distribution (Rubin et al., 2004) or the lamellae arrangement (Fratzl et al., 2004; Weiner & Traub, 1992; Weiner et al., 1999).

An example of a healthy mouse vertebrae imaged with scanning electron microscopy is presented in Figure 3c). For trabecular bone some structural parameters can be defined such as the area occupied by trabeculae, inter-trabecular distance and the trabecular thickness. Image analysis software, as Sigma ScanPro or Image J, can be used to determine the parameters mentioned (Caetano-Lopes et al. 2009a, 2010).

While the images of Figure 3b) to e) were obtained with secondary electrons (SE), backscattered electrons (BSE) can also be used and images of Figure 4 are an example. Figure 4a) and b) are respectively images from control and from osteoporotic vertebral L4 trabecular bone mice. The arrangement of lamellae can be observed (Figure 4).

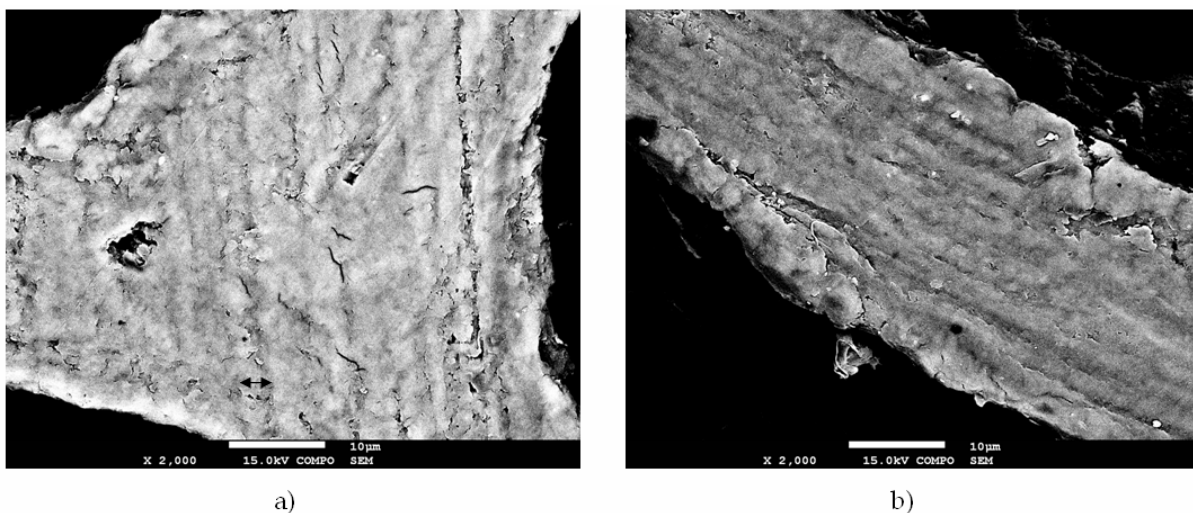


Fig. 4. Images of SEM with backscattered electrons: a) from a control and b) from an osteoporotic mice vertebral L4 trabecular bone. Lamellae can be observed, and on figure a) a black arrow indicates a lamellae

#### 2.4.3 Second-harmonic generation SHG and two-photon excitation microscopy

Second-harmonic generation (SHG) and two-photon excitation microscopy is used to evaluate the collagen organization of bone (Caetano-Lopes et al., 2009a, 2010). Collagen is

able to generate a second-harmonic signal due to the nonsymmetrical arrangement (Cox et al., 2003; Cox & Kable, 2006). When an electric field is able to deform a molecule, a second-harmonic generation occurs. With collagen, an asymmetrical molecule, an oscillating field is generated at twice the frequency (second-harmonic). Prior to observation, bone samples are decalcified, embedded in paraffin, cut in a microtome and deparaffinized. With this technique it is possible to distinguish the mature polymerized collagen from the immature collagen, indicating fibrillogenesis. The backward-SHG channel detects the backscattered-SHG signal associated to a green image, representing a less dense and immature collagen network, while the forward-SHG channel captures forward-SHG signal originating a blue image, associated with presence of a more dense and polymerized collagen matrix. Image analysis software is used to determine the amount of mature and immature collagen on a given area. The relative distributions of mature and immature collagen were found to be equivalent in the arthritic and control groups of 5 months old SKG mice (Caetano-Lopes et al., 2009a). However, in the 8 months old SKG mice, we have observed that the ratio of the forward to backward signal was higher in arthritic animals than in control, which revealed a lower collagen density and organization (Caetano-Lopes et al., 2010). As an example, Figure 5 shows two multiphoton microscopy images from a) SKG mouse vertebrae and b) BALB/c mouse vertebrae. The collagen component is strongly affected by the inflammatory disease which was eventually reflected on the mechanical performance of bone.

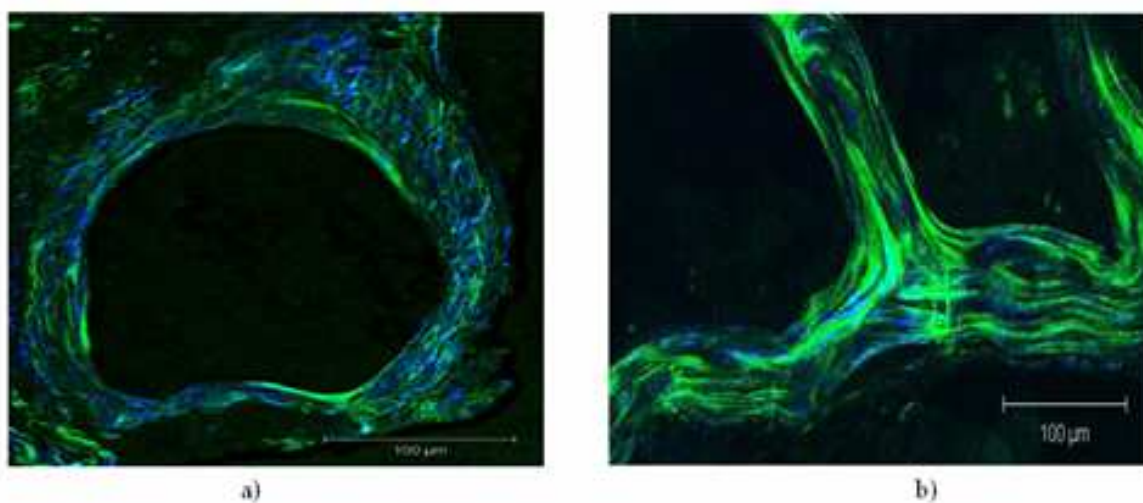


Fig. 5. Multiphoton microscopy images from 5 months old a) arthritic and b) control vertebrae of mice. Green and blue colors correspond respectively to the backward- and forward-SHG channels

#### 2.4.4 Microcomputed tomography (micro-CT or $\mu$ -CT)

Microcomputed tomography (micro-CT) is a technique that enables to characterize bone microstructure. It has been used to evaluate bone volume fraction or apparent density, as well as the architectural bone arrangement (Cory et al., 2010; Nazarian et al., 2007). Micro-CT has becoming a leading technique on non-destructive structural evaluation.

Three-dimensional (3D) micro-CT has been applied to the visualization and quantification of the 3D structure of trabecular bone (Bevill et al., 2009; Chappard et al., 2008; Chevalier et al., 2007; Diederichs et al., 2009; Ding et al., 1999; Djuric et al., 2010; Homminga et al., 2002; Jiang et al., 2003; Link et al., 1998; Macho et al., 2005; Teo et al. 2006; Teo et al. 2007). Micro-

CT may be used to evaluate differences of trabecular microstructure, for example between several age groups (Djuric et al., 2010; Macho et al., 2005) at different femoral regions (Bevill et al., 2009; Djuric et al., 2010), or on vertebral bodies (Teo et al. 2006).

The identification of the optimal micro-CT parameters for human trabecular bone characterization has been performed by the authors of this chapter (Pereira et al.). Acquisition (voltage, intensity), resolution (voxel size), and especially image analysis (threshold values) parameters, were adapted in order to optimize the experimental procedures. Our experience has been centred in samples from patients with osteoarthritis and osteoporosis, who were submitted to total hip arthroplasty. The removed hip epiphysis were subjected to drilling, fixation, dehydration, cleaning and, in some of the cases, impregnation.

Micro-CT procedure involves three main steps: acquisition, reconstruction and image analysis. During the acquisition step, scans are performed in order to obtain, for each sample, a stack of about 500 images. On the reconstruction phase, the binarization is carried out, that is, to separate bone from regions without bone tissue and thresholding or other segmentation methods may be used for the definition of Bone Volume of Interest (BVI). To reconstruct the images, a 3D reconstruction software is used to generate an assemblage of virtual cross section slices through the object. Figure 6 shows the scanned image, the Bone Volume of Interest (BVI), the binarized region, and the 3D rendering (*i.e.*, manipulation in a virtual space) of a sample of a human trabecular bone. Figure 7 exhibits a 3D reconstruction image of an equine cortical bone.

On the third phase, the image data is interpreted with 3D analysis software, which enables the quantification of the parameters that characterize the trabecular bone structure (Parfitt et al., 1987): Percent bone volume (BV/TV, %), Bone specific surface (BS/BV,  $\text{mm}^{-1}$ ), Bone surface density (BS/TV,  $\text{mm}^{-1}$ ), Structure Model Index (SMI, none), Trabecular thickness (Tb.Th, mm), Trabecular number (Tb.N,  $\text{mm}^{-1}$ ), Trabecular separation (Tb.Sp, mm) and Degree of anisotropy (DA, none).

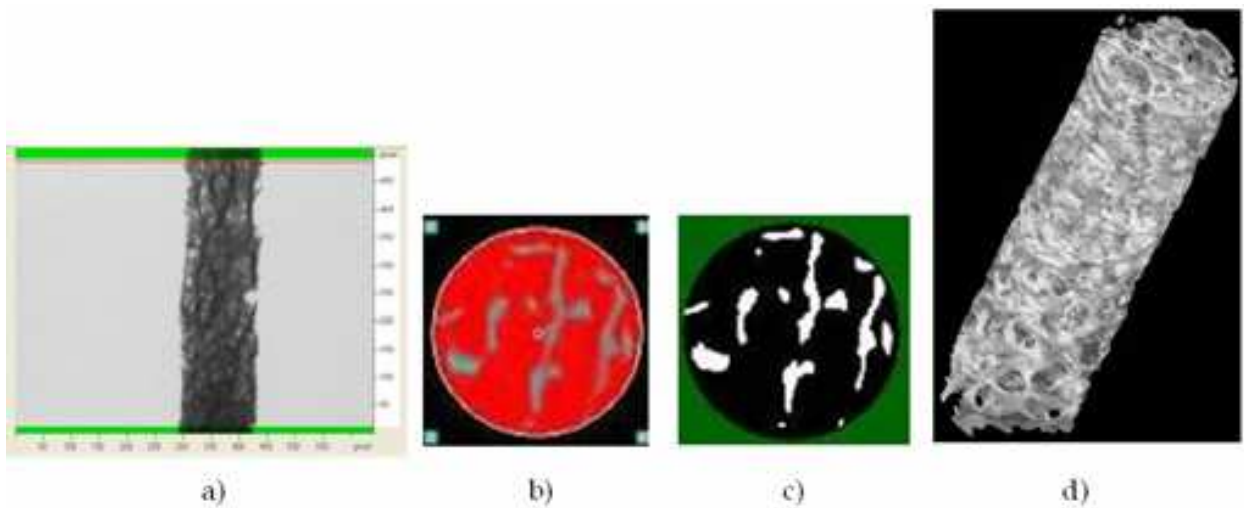


Fig. 6. a) Projection Image, b) Bone Volume of Interest (BVI), c) Binarized BVI, d) 3D rendering

Although most of the work on the application of micro-CT is for trabecular bone, cortical bone has also been studied (Basillais, 2007; Cooper et al., 2007a, 2007b; Wachter et al., 2001). For cortical bone characterization, the used parameters are (Parfitt et al., 1987): Canal volume fraction (Ca.V/TV), Pore volume fraction (Po.V/TV), Surface to volume ratio

(Ca.S/Ca.V), Mean diameter of pores (Ca.Dm), Mean pore separation (Ca.Sp) and Degree of anisotropy (DA).

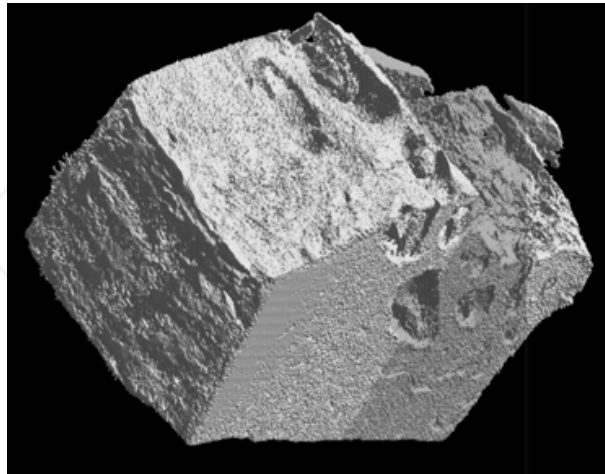


Fig. 7. Three-dimensional (3D) reconstruction image of an equine cortical bone

#### 2.4.5 Quantitative backscattered electron imaging, qBEI

The mineralized component of bone is directly related to the fragility of bone. In this way, it is extremely important to determine the volume fraction of mineral particles, their shape and arrangement (Fratzl et al., 2004). The average mineral content of bone is in the range of 30 to 55%, but the trabeculae in the trabecular bone or the osteons in the compact bones do not exhibit a uniform mineralization. In fact, they have a regional variation (Fratzl et al., 2004). Two factors contribute to this difference in the degree of mineralization (Fratzl et al., 2004). One factor is remodeling as the old matrix is continuously resorbed and replaced by new bone. The other factor is related to the fact that mineralization of the matrix follows a certain time course, including a rapid mineralization within a few days combined with a mineralization that takes years. As a result, bone is formed by different zones which have distinct mineral characteristics, with the lower mineralized zones corresponding to fresh bone formation (Fratzl et al., 2004). The mineral content in different zones may be determined by quantitative backscattered electron imaging, qBEI (Fratzl et al., 2004) as explained schematically with the help of Figure 8a). The qBEI method is used to obtain the bone mineralization density distribution (BMDD), which can be represented by the scheme of Figure 8b) (Fratzl et al., 2004). BMDD provide complementary data to BMD (bone mineral density) for osteoporosis diagnosis and management.

The qBEI is based, on the detection of backscattered electrons, using SEM. As previously mentioned the intensity of backscattered electrons increases with the atomic number. Bone is essentially formed by the organic matrix, which is composed by the elements H, C, N, O, P, S and by a mineral phase, which has Ca, P, O, H, C and Mg as components (Roschger et al., 1998). From these elements, Ca is the one with the highest atomic number and as a result it dominates the intensity of the backscattered beam.

The sample preparation involves dehydration and embedding the bone sample into polymethylmethacrylate, followed by polishing (Roschger et al., 1998).

In qBEI technique, different gray levels are correlated with different calcium contents (Fratzl-Zelman et al. 2009; Roschger et al., 1998, 2008, 2010). To achieve this effect, first, the backscattered signal is calibrated using the atomic number contrast of the reference

materials, carbon and aluminum. Secondly, calibrated gray levels must be converted into calcium concentration, taking 0% of Ca for osteoid and 39.86% Ca for pure hydroxyapatite (Roschger et al., 1998). From the bone mineralization density distribution (BMDD) curves (see Figure 8b)), the following parameters can be determined:  $Ca_{\text{mean}}$  (the weighted mean calcium concentration),  $Ca_{\text{peak}}$  (the peak of the calcium concentration),  $Ca_{\text{width}}$  (the width at half of the calcium distribution),  $Ca_{\text{low}}$  (the percentage of bone area that is mineralized below 5%) and  $Ca_{\text{high}}$  (the percentage of bone area that is mineralized above 95%) (Roschger et al., 2008, 2010). Patients with pathological remodeling disturbances present different parameters in comparison with healthy individuals (Roschger et al., 1998).

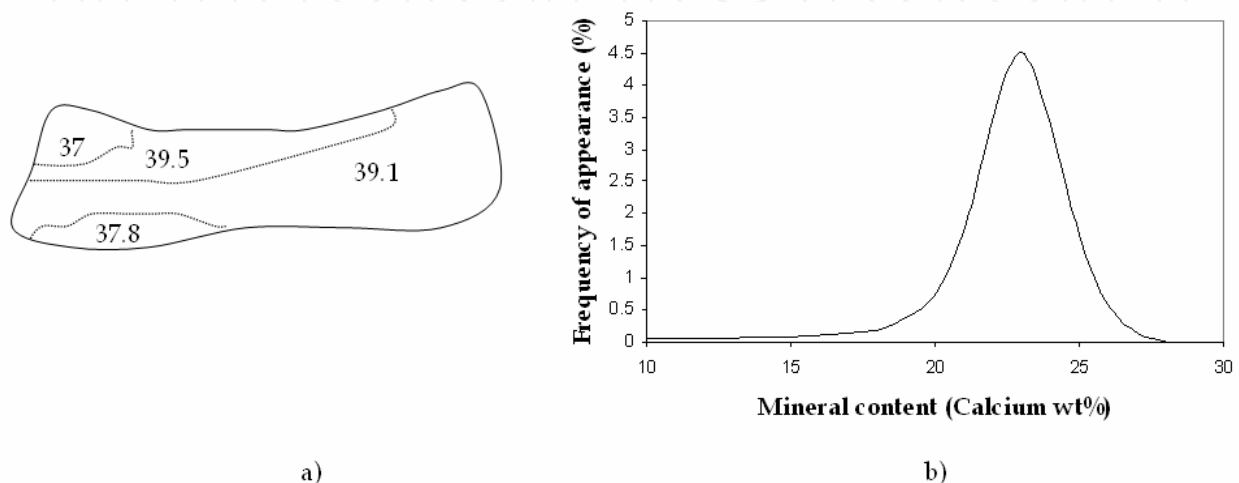


Fig. 8. a) Different zones with different mineral content, b) bone mineralization density distribution (adapted from (Fratzl et al. 2004))

#### 2.4.6 Atomic force microscopy AFM

Atomic force microscopy (AFM) can be used to assess the structure and the topology of bone (Bozec et al., 2005; Fantner et al., 2004; Hassenkam et al., 2004) and also to evaluate the mechanical properties of the constituents by nanoindentation, which will be described in section 3.

AFM is based into a piezo mechanism, on which the deflection of an arm, due to van der Waals forces between the atom of the tip and the atom at the surface, is measured.

The sample preparation procedure is simple and only involves bone marrow removal and dehydration. The sample is glued to metal disks (Fantner et al., 2004; Hassenkam et al., 2004).

Studies on structural or morphological characterization of bone with AFM were carried out either for trabecular (Fantner et al., 2004; Hassenkam et al., 2004, 2006; Hengsberger et al., 2001) and for cortical bone (Bozec et al., 2005; Hengsberger et al., 2001). For example, AFM imaging of the surface of trabecular bone reveals the arrangement of either the collagen fibres as well as the crystals distribution, which can be used to assess the role of the two components at the nanoscale level (Hassenkam et al., 2004). The mineral phase was found to have a platen shape and lies flat on the fibrils (Hassenkam et al., 2004). In animals, AFM showed that on the surface of a trabecula there is a woven layer of less mineralized fibrils in comparison with the trabecular interior where the mineral phase is higher (Hassenkam et al., 2004). Also, the arrangement of mineralized collagen around an osteon can be observed by AFM (Bozec et al., 2005).

#### 2.4.7 Small angle X-ray scattering, SAXS

The thickness of bone mineral plates is difficult to evaluate from X-ray diffraction data, but can be extracted from small-angle X-ray scattering. In this method, the scattering of X-rays by a sample is recorded at low angles. The technique is used to analyze the size and shape of mineralized particles, as well as their distribution (Bunger et al., 2010; Fratzl et al., 2004; Fratzl-Zelman et al. 2009; Roschger et al., 2010).

The scattered intensity and the scattering vector are obtained and converted into shape parameters (Bunger et al., 2010; Fratzl et al., 2004; Roschger et al., 2010). In bone analysis, the SAXS parameter  $T = 4\Phi(1 - \Phi) / \sigma$ , where  $\Phi$  is the mineral bone volume fraction and  $\sigma$  is the bone surface per unit volume is used to estimate the average mineral particles thickness (Fratzl et al., 2004; Fratzl-Zelman et al. 2009; Roschger et al., 2010). It is assumed that the mineral particles have the shape of platelets. A shape function  $G(x)$  can also be derived from the SAXS data to characterize the mineral particle shape, size distribution and arrangement (Fratzl et al., 2004). The shape function exhibits differences between different species, like human and rat (Fratzl et al., 2004). Another example is the examination of bone from normal and ovariectomized rats by SAXS which found that the mineral plates were thicker in old bone in comparison with new bone (Bunger et al., 2010).

#### 2.4.8 Neutron scattering

The mineral-matrix arrangement has an extremely important impact on the bone properties and some of the matrix properties can be extracted from neutron scattering experiments.

The fibrils, *i.e.*, the molecules of mineralized collagen are arranged in a banded structure as previously stated. Neutron scattering experiments can be used to determine the spacing between adjacent collagen molecules or adjacent fibrils. It was shown that the spacing between collagen molecules was 1.6 nm and 1.1 nm respectively for non-mineralized wet and dry molecules, while for the mineralized wet bone, the distance between adjacent fibrils was 1.25nm (Fratzl et al., 2004; Fratzl & Weinkamer, 2007).

### 2.5 The effect of disease on the bone's structure

Metabolic bone diseases and inflammatory rheumatic diseases will be considered.

#### 2.5.1 Metabolic bone diseases

Osteoporosis (OP) is a bone disease defined as a systemic skeletal disease characterized by a reduction in bone mass and microarchitectural deterioration of bone tissue, which leads to an increased bone fragility and susceptibility to fracture (Kanis et al., 2005).

Bone microarchitecture deterioration occurs due to changes in organic matrix and a decrease in the mineralized component of bone (Boyle et al., 2003). This effect occur when the balance between bone formation and bone resorption is disrupted by increased resorption (*i.e.* menopause) or decreased formation (*i.e.* aging).

Bone mass loss is not due to exactly equal mechanisms in men and women. While in men, bone loss predominantly occurs by trabecular thinning and reduced bone formation, in women there is an earlier loss of connectivity between trabeculae and earlier cortical thinning (Seeman, 2007).

The comparison of normal with osteoporotic human bone shows a decrease in the trabeculae thickness and a deficiency in the trabecular structure with breakage of trabeculae (Rubin et al., 2004).

It was found that the removal of struts or loss of connectivity reduces more severely the modulus of elasticity and the strength than the uniform thinning (Fratzl, & Weinkamer, 2007; Gibson, 2005).

The techniques described above can detect differences between normal and osteoporotic bones and are very useful as research tools to study animal model and human bone samples.

### 2.5.2 Inflammatory rheumatic diseases

Inflammatory systemic diseases like rheumatoid arthritis (RA) are characterized by chronic inflammation, which induces synovium proliferation, increasing local and systemic bone resorption and ultimately structural damage and secondary OP (Alamanos & Drosos, 2005; Caetano-Lopes et al., 2009b; Orstavik et al., 2004; van Staa et al., 2006). Osteoimmunology is a new research field, which bridges the concepts of inflammation and bone.

The study of the effect of rheumatoid arthritis (RA) on the structure of bone is not a simple task. In fact patients who suffer from RA are submitted to medications which may contribute to bone fragility. In this way, the use of a mice model to study the effect of chronic inflammation on the structure of bone is useful (Caetano-Lopes et al., 2009a, 2010) and recently we have studied the inflammation on bone using the SKG mice model, which behaves like human RA (Caetano-Lopes et al., 2009a, 2010). SKG mice were obtained from BALB/c mice, with a point mutation in the ZAP-70 gene, which triggered by a zymosan injection developed a chronic arthritis (Caetano-Lopes et al., 2009a, 2010). BALB/c can be used as control for SKG mice.

In five months (Caetano-Lopes et al., 2009a) and eight months (Caetano-Lopes et al., 2010) arthritic SKG mice, we have evaluated the bone structure by scanning electron microscopy and found that it was affected by the inflammatory disease. For example, the trabecular thickness was reduced from  $70.91 \pm 23.66$  to  $57.18 \pm 16.78$   $\mu\text{m}$  in arthritic animals (Caetano-Lopes et al., 2009a). The vertebrae from arthritic mice have a higher inter-trabecular distance and a decreased trabeculae thickness (Caetano-Lopes et al., 2009a, 2010).

At higher magnifications, the structure of lamellae can be observed by SEM with backscattered electrons (Figure 4). Comparing Figures 4a) and b), respectively from control and osteoporotic mice, no particular differences can be detected with this technique, at this scale range.

In an inflammatory process the lack of collagen matrix repair affects the mineral crystal deposition, which will contribute to the decreasing of mechanical strength (Caetano-Lopes et al., 2010).

## 3. Mechanical properties

This chapter gives an emphasis on the relationship between the complex hierarchical structure of bone and its mechanical properties. Bone is a complex but ordered composite material having the function of resisting to mechanical forces and fractures.

With regard to the assessment of the bone stiffness, strength and toughness, there are different tests such as compression, tension, bending, fatigue, creep, torsion and nanoindentation.

In addition, these tests can be performed under different loading conditions, alone or in combination, and can be applied either cyclically or monotonically, short- or long-term, and at several loading rates. At a more microscopic level, atomic force microscopy may be used

for nanoindentation, which measures the mechanical properties of the bone units, trabeculae or osteons, respectively for trabecular and cortical bone.

In the mechanical tests, it is possible to obtain data that enables the assessment of parameters like the elastic or Young's modulus, the yield stress, and energy until yield which are used to evaluate respectively the stiffness, strength and toughness of bone. An example of a stress-strain compression curve is given in Figure 9c), where an indication of these parameters is shown. The Young's modulus is the slope of the stress-strain curve in the elastic regime. The yield stress is the stress attained at the end of elastic deformation and the energy until yield is evaluated by the area under the curve before yielding (Viguet-Carrin et al., 2006).

Several factors affect the mechanical properties of bone, such as, age (Sun et al., 2008; Wang et al., 2002, 2005; Woo et al., 2010), sex (Duan et al., 2005; Seeman, 2003, 2007; Wang et al., 2005), anatomical location (Morgan & Keaveny, 2001; Morgan et al., 2003; Nazarian et al., 2007), load orientation (Fratzl, & Weinkamer, 2007; Gibson & Ashby, 1999; Gibson, 2005), geometry/architecture (Ammann & Rizzoli, 2003; Rho et al., 1998; Silva, 2007), arrangement of collagen fibers and mineral particles (Viguet-Carrin et al., 2006), bone density (Ammann & Rizzoli, 2003; Cory et al., 2010; Kopperdahl & Keaveny, 1998; Mueller et al., 2009; Silva, 2007), and bone diseases (Caetano-Lopes et al., 2009a; Ciarelli et al., 2000; Homminga et al. 2002; Li & Aspden, 1997; Sun et al., 2008; Woo et al., 2010).

The arrangements of bone trabeculae, the orientation of collagen fibres and carbonated apatite crystals in relation to load have an important role in determining bone strength (Viguet-Carrin et al., 2006). Carbonated apatite crystals are very stiff and strong, but not very tough, with a Young's modulus around 165 GPa, while collagen has much more toughness but is not very stiff, and exhibits a modulus of 1.24 GPa. The mechanical properties of bone depend on the arrangement of collagen fibers which condition the deposition of mineral crystals and influences bone strength (Viguet-Carrin et al., 2006). The composite, remarkably combines, the properties of the two components, the stiffness and the toughness. As for any other composite material, the elastic modulus of the bone will have an intermediate value between the ones of its components.

Woven bone composed by unorganized collagen fibers has lower mechanical properties than lamellar bone with a well defined arrangement of mineralized collagen fibers, which reveals the importance of the collagen disposition (Viguet-Carrin et al., 2006).

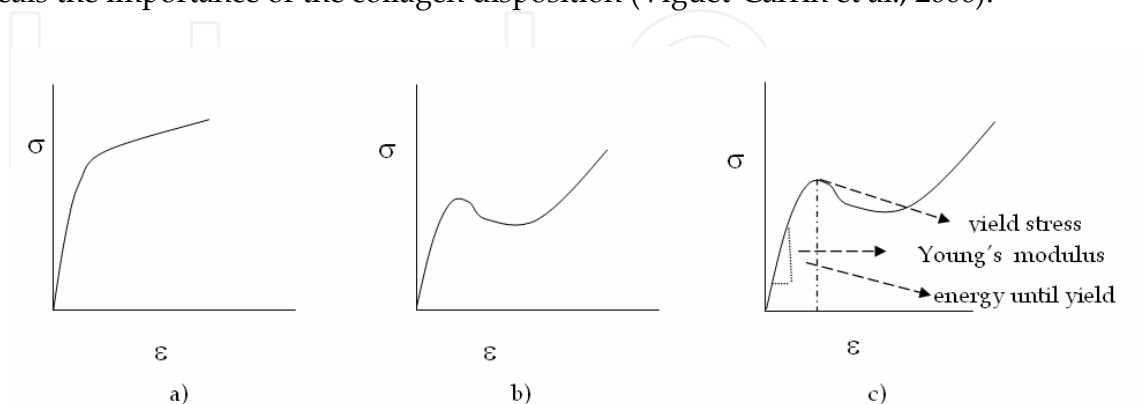


Fig. 9. Schematically compressive stress-strain curves for healthy a) cortical and b) trabecular bone (adapted from (Gibson & Ashby, 1999)), c) typical stress-strain curve with the indication of the Young's modulus, yield stress and energy until yield (adapted from (Viguet-Carrin et al., 2006))

While cortical bone has a Young's modulus in the range of 10 to 20 GPa, the trabecular bone has a lower value of the stiffness, with values that can vary between 0.3 and 3000 MPa (Fung, 1993).

It is widely accepted that the relative density of trabecular bone depends on the load that it suffers, with low density structures developing where the stress is low. In this sense, the trabecular architecture adapts to the external loading (Fratzl, & Weinkamer, 2007; Gibson & Ashby, 1999; Gibson, 2005; Keaveny et al., 2001). If the loads are equivalent in the three directions of bone, a structure with equiaxed cells is obtained. However, if load is higher in one direction, the trabeculae tend to align in the load direction, adopting an anisotropic structure (Gibson & Ashby, 1999; Keaveny et al., 2001).

In cortical bone the mechanical properties depend on the porosity, degree of mineralization and organization of bone (Rho et al., 1998) and at a macroscopic level properties vary from one bone region to another (Rho et al., 1998). In human trabecular bone, the mechanical properties change from the periphery to the center of the bone (Rho et al., 1998). The intrinsic mechanical properties of isolated osteons and individual trabeculae can be determined. The elastic modulus of single trabeculae was found to be similar to the one of the cortical tissue (Rho et al., 1998).

Although sometimes it is not taken into account, hydration is also an important factor which has to be considered when performing mechanical tests of bone. It is known that dry bone has a higher Young's modulus, but the strength and strain to failure decrease significantly (Gibson & Ashby, 1999). Thus, the mechanical tests are generally performed with wet bones. This section will be divided in subsections, for specific types of mechanical tests. The influence of some parameters on those types of tests will be also addressed. Some issues related with bone deformation mechanisms will be discussed in section 3.8, while the effect of aging and disease on the bone's mechanical properties will be handled on section 3.9.

### 3.1 Compression

The compression tests are the most frequently performed tests to determine the bone's mechanical properties, due to their simple procedure and to the fact that bones are often submitted to compression loads (Cory et al., 2010; Kopperdahl & Keaveny, 1998; Li & Aspden, 1997; Morgan & Keaveny, 2001; Morgan et al., 2003; Sun et al., 2008; Woo et al., 2010).

The mechanical behaviour of cortical bone is quite different from the behaviour of trabecular bone, as schematically presented in the stress-strain curves of Figure 9a) and b) (Gibson & Ashby, 1999). The cortical bone tested in the longitudinal direction exhibits an elastic region up to strains of 0.7% and a plastic deformation until 3% (Gibson & Ashby, 1999). Bone has an anisotropic performance, as when is tested along the transversal direction is less stiff and strong (Gibson & Ashby, 1999).

In the present chapter, more relevance will be given to trabecular bone, due to its importance from the clinical point of view. Trabecular bone is included in the class of open cellular materials or foams. The compressive stress-strain curves of healthy trabecular bone are characterized by three distinct regions (Figure 9b)) (Gibson & Ashby, 1999; Gibson, 2005). The initial elastic response is due to the bending of trabeculae, while the second region is associated with elastic buckling, plastic yielding or brittle fracture of trabeculae (Gibson & Ashby, 1999). Finally the third regime occurs when cell walls or trabeculae touch each other (Gibson & Ashby, 1999). It is generally accepted that the mechanical properties of

trabecular bone are related to their density. For example, the Young's modulus is proportional to the square of the relative density (Gibson & Ashby, 1999; Gibson, 2005).

Several works can be found on the compression of trabecular bone, using vertebrae (Ammann & Rizzoli, 2003; Kopperdahl & Keaveny, 1998; Matsuura et al., 2008; Morgan & Keaveny, 2001; Morgan et al., 2003; Silva, 2007; Woo et al., 2010), tibia (Fonseca & Ward, 2004; Morgan & Keaveny, 2001; Morgan et al., 2003), femur (Cory et al., 2010; Fonseca & Ward, 2004; Morgan & Keaveny, 2001; Morgan et al., 2003) and femoral heads (Ciarallo et al., 2006; Knoob et al., 2007; Li & Aspden, 1997; Matsuura et al., 2008; Morgan & Keaveny, 2001; Morgan et al., 2003; Sun et al., 2008). For example, it was found that for a given density, samples from tibia had higher Young's modulus than the ones from vertebrae (Morgan et al., 2003).

Experimentally, the compression of bone can be performed either in animal model or in human samples.

We have used a mice model, the SKG arthritic mice, to evaluate the effect of chronic inflammation on the biomechanical properties of the bone (Caetano-Lopes et al., 2009a). Compression tests on the vertebral bodies of SKG mouse chronic arthritis model were performed (Caetano-Lopes et al., 2009a, 2010). In this case, a load cell of 500N and a cross-head speed of 0.01 mm/s were used. Samples were kept wet during the test. From the load F - displacement  $\Delta L$  curves, stress and strain are calculated, respectively, as

$$\sigma = F/A \quad (1)$$

$$\varepsilon = \Delta L/L \quad (2)$$

where A is the sample area and L is the length. The stress-strain curves of Figure 10 were calculated assuming that the vertebrae have a cylinder body. Figure 10a) and b) shows the stress-strain curves obtained on the compression of arthritic and control female 5 months mice vertebrae. A photograph with the vertebrae can be observed in Figure 10c). Parameters like the elastic modulus, yield stress, maximum stress, energy until yield and the energy until maximum stress were determined. SKG mice vertebrae were found to exhibit lower stiffness, strength and toughness in comparison with the results obtained on the compression of control BALB/c mice, aged 5 and 8 months (Caetano-Lopes et al., 2009a, 2010).

Compression of trabecular bone samples from femoral epiphyses collected from patients with osteoporosis and osteoarthritis was performed by this chapter's authors (Vale et al.). Figure 11 shows a cylinder of trabecular bone, the compression set-up used and the stress-strain curve obtained on the compression test of a human sample from a patient with osteoporosis.

The methodology of the compression tests is not always the same and variables like the geometry, dimensions of the samples and type end supports can vary. The shape of the samples may be cubic (Diamant et al., 2007; Sun et al., 2008) or cylinder (Li & Aspden, 1997; Matsuura et al., 2008; Morgan & Keaveny, 2001). In general, cylinders are more used as they are easily obtained by drilling. From several studies, it is suggested that cylinder specimen with a length: diameter ratio between 1.5 and 2 provides accurate results (Li & Aspden, 1997; Matsuura et al., 2008; Morgan & Keaveny, 2001). The sample in Figure 11 is in this range of ratio, with a diameter of 15 mm.

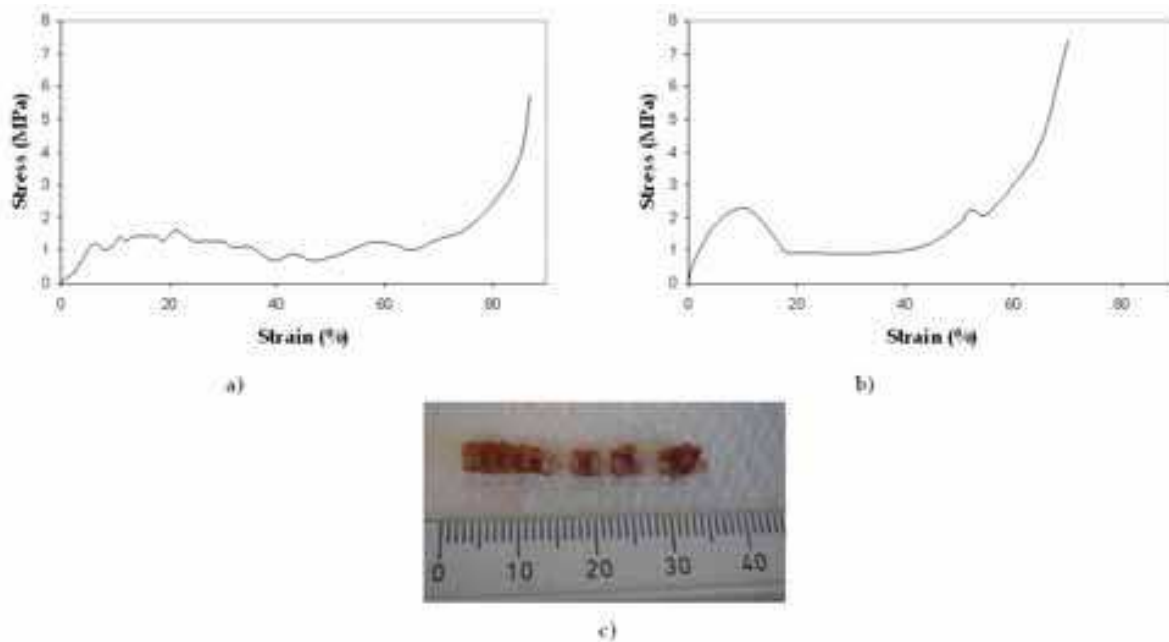


Fig. 10. a) Stress-strain curves obtained on the compression of a) arthritic and b) control female 5 month mice vertebrae. c) Photograph of mice vertebrae

While in some publications, it is not clear the type of end support used, on other cases it is mentioned the platen technique and the end-cap technique. In the platen method the samples are placed inside metallic platens (Helgason et al., 2008; Morgan & Keaveny, 2001), while with the end-cap method the samples are embedded into polymeric end-caps (Helgason et al., 2008; Matsuura et al., 2008; Morgan & Keaveny, 2001). Both methodologies intend to minimize the side effects, but it is not consensual which the most reliable procedure is. We have used a metallic platen for the upper extremity of the sample, while the bottom was left free.

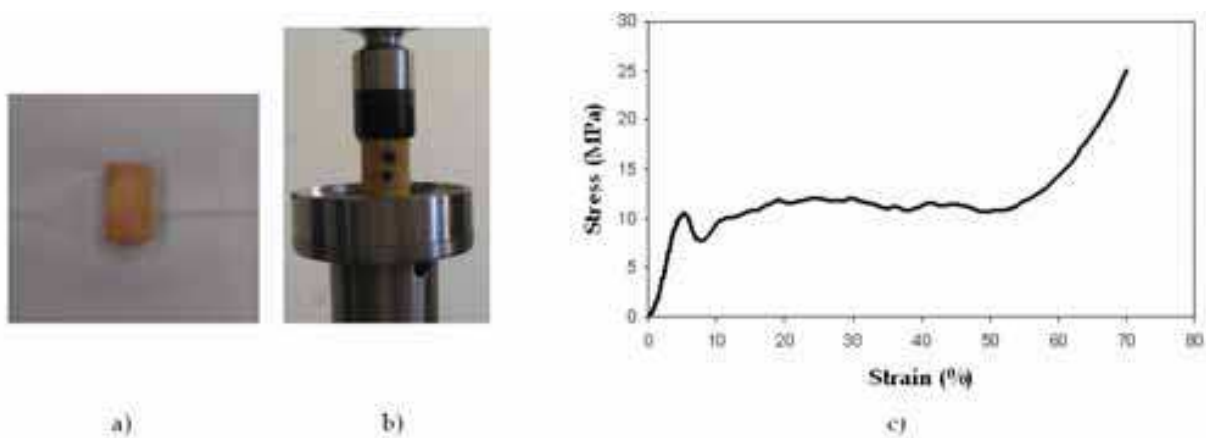


Fig. 11. a) Cylinder of trabecular bone, b) compression set-up and c) stress-strain curve for a human sample from a male patient with osteoporosis

### 3.2 Tension

The preparation of specimens to perform tensile tests is not simple; probably this is one of the reasons why the studies on bone traction are rarer. For example, the extremities of a

mice femur may be inserted in brass fixtures and glued with dental cement, followed by bone micromachining (Ramasamy & Akkus, 2007). Other authors mentioned that cylindrical specimens from human trabecular bone were embedded into polymeric end-caps to fit into the grips of the testing machine (Morgan & Keaveny, 2001).

Tensile stress- strain curves for healthy trabecular bone are characterized by an initial linear elastic region, followed by a non-linear deformation until a maximum is achieved which corresponds to crack initiation (Gibson & Ashby, 1999). In tension, the Young's modulus of the compact bone increases with the mineral content (Giraud-Guille, 1988).

The tensile-compressive yield strength ratio is around 0.62 for trabecular bone (Bayraktar et al., 2004). This means that the strength is asymmetric, with a higher strength in compression than in tension. The difference between tensile and compression curves can be observed in the plots of Figure 12, for mice femur, for which the compression strength is greater than the tensile strength (Ramasamy & Akkus, 2007). The Young's modulus is also higher in compression than in traction, either in vertebrae, tibia and femoral heads (Morgan & Keaveny, 2001).

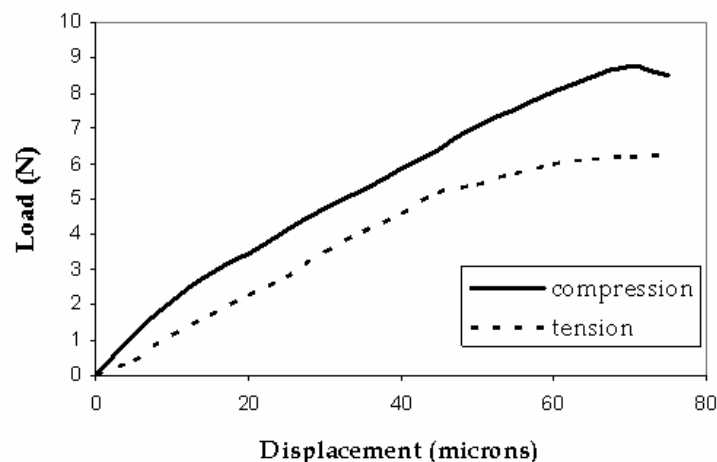


Fig. 12. Comparison of the load-displacement curves obtained in tension and in compression for mice femur (adapted from (Ramasamy & Akkus, 2007))

### 3.3 Bending

The mechanical performance of the entire bone is of much interest from the clinical point of view and bending tests are the most common methods used to analyze long bones as a whole (Sharir et al., 2008).

Bending tests can use three or four point bending devices (Sharir et al., 2008). In a three point bending test, the bone is placed on two supports, while only one support contacts the opposite surface, exactly at the mid point between the two supports. In this case, the maximum load occurs at the middle point and the bone will fracture in this location (Sharir et al., 2008).

On the four point bending procedure, there are two upper and two lower supports. The advantage is that the section of the bone is submitted to a uniform moment, without shear effects (Sharir et al., 2008). However, as bones have an irregular geometry, it is difficult to have two supports contacting bone at the same time. In addition, samples may have a size too small for this technique. Due to these reasons, the three point bending procedure is the most used for bone (Sharir et al., 2008).

To calculate the stresses and strains during the test, it is assumed that bones are cylinders and the diameter of their cross section is  $d$ . The applied load is denoted by  $F$ ,  $S$  is the distance between lower supports and  $\Delta l$  is the elongation of the sample. Therefore the stress and the strain are given respectively by (Beer et al., 1992)

$$\sigma = \frac{FS}{\pi \left(\frac{d}{2}\right)^3} \quad (3)$$

$$\varepsilon = \frac{12 \left(\frac{d}{2}\right) \Delta l}{S^2} \quad (4)$$

Bending tests may be performed with animal radius, femurs and tibias (Akhter et al., 2001; Bensamoun et al., 2006; Schriefer et al., 2005; Shahnazari et al., 2007) to determine bone strength. For the evaluation of bending data, it is usual to define yield stress, Young's modulus, ultimate stress, ultimate strain and energy until the maximum stress (Akhter et al., 2001; Bensamoun et al., 2006; Schriefer et al., 2005).

We have performed three point bending tests with femoral bones of SKG and BALB/c mice at a cross-head speed of 0.01 mm/s and a load cell of 500N (Caetano-Lopes et al., 2009a, 2010). Figure 13 shows stress-strain curves obtained from the bending of arthritic and control female mice femurs, as well as the experimental set-up for three point bending of mice femur. The distance between supports is 5mm. From the stress-strain curves it was possible to obtain the above mentioned parameters. The results obtained showed that arthritic femurs had, in comparison with control animals, lower elastic modulus, yield stress, ultimate stress and energy until ultimate stress.

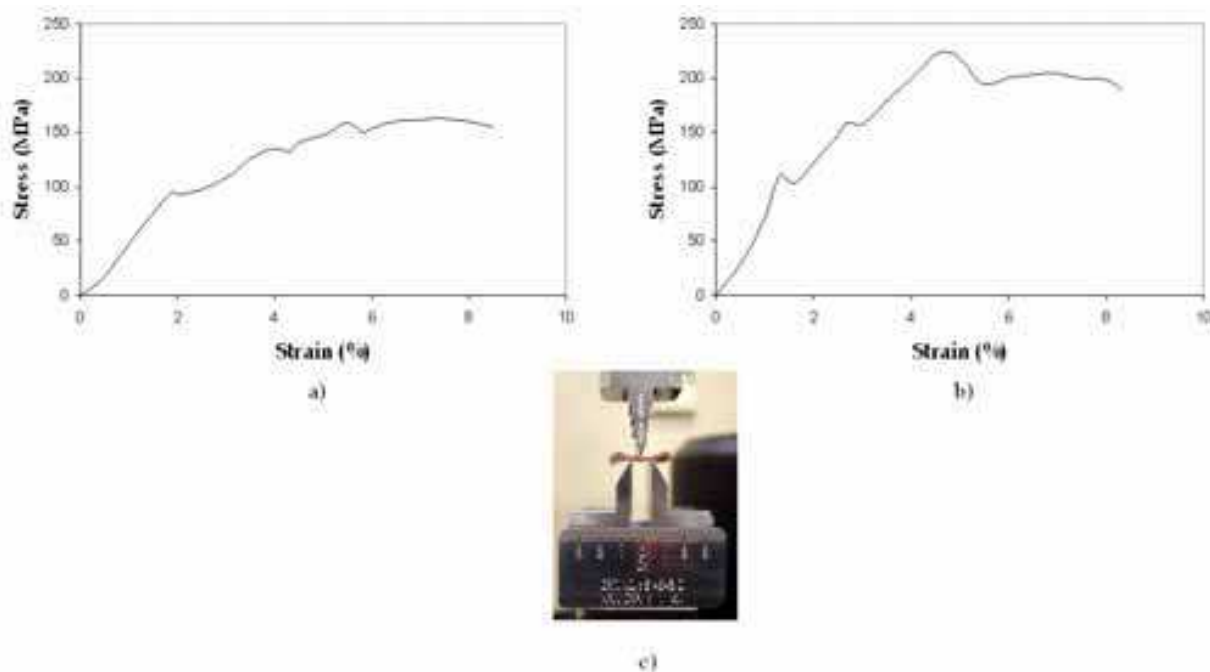


Fig. 13. a) Stress-strain curves obtained on the bending of a) arthritic and b) control female 5 month mice femurs, c) experimental set-up for three point bending of mice femur

### 3.4 Fatigue

Bones are subjected to fatigue due to the action of cyclic loading. Some studies can be found in the literature on fatigue of human trabecular bone (Dendorfer et al., 2008; Haddock et al., 2004; Rapillard et al., 2006; Yamamoto et al. 2006), but the majority of the works describe results from animal testing (Dendorfer et al., 2008, 2009; Ganguly et al., 2004; Haddock et al., 2004; Moore et al., 2003; Moore & Gibson, 2003).

A material under cyclic loading fails at stresses below the values that the material can bear under static loading. Bones are subjected to fatigue loading as a result of daily activity or prolonged exercise, which occurs for instance in athletes (Ganguly et al., 2004; Moore et al., 2003; Moore & Gibson, 2003). Fatigue loading is one of the primary causes of human bone failure (Ganguly et al., 2004). Therefore, it is important to characterize the residual strains that occur after cyclic loading (Yamamoto et al., 2006).

Fatigue fractures may occur in young adults (failure due to stress concentration, known as stress fractures). Failures due to stress concentration result from prolonged exercise and occur more frequently at the tibia and metatarsal bones, while fragility or osteoporotic fractures of elderly individuals take place on the proximal femur and on vertebrae where the trabecular bone supports most of the load (Ganguly et al., 2004).

Fatigue damage results from accumulation of micro-cracks (Fratzl & Weinkamer, 2007; Moore et al., 2003; Taylor, 1998). Micro-cracks are repaired through bone remodeling. However, if micro-cracks are not repaired, they accumulate and coalesce, leading to a decrease in bone stiffness and to an increase of fracture risk (Dendorfer et al., 2008; Moore et al., 2003; Moore & Gibson, 2003; Taylor, 1998).

The preparation of bone samples to perform fatigue tests includes an initial defatting of cylinder specimens, followed by a press-fit into brass end caps of the sample extremities (Dendorfer et al., 2008; Ganguly et al., 2004; Moore et al., 2003; Moore & Gibson, 2003; Yamamoto et al., 2006). The extension may be measured by extensometers attached to the brass caps (Ganguly et al., 2004; Moore et al., 2003; Moore & Gibson, 2003) or by the displacement of the cross-head (Dendorfer et al., 2008). As fatigue tests may take a long time, samples must be kept wet with soaked gauze or using a saline bath (Dendorfer et al., 2008; Ganguly et al., 2004; Moore et al., 2003; Moore & Gibson, 2003).

Fatigue tests consist on the application of a certain number of cycles of compressive loading and unloading. As an initial step, samples are subjected to a small number of cycles (10 cycles) with low stress and strain. The initial secant elastic modulus  $E_0$  is determined from the slope of the 10<sup>th</sup> cycle (Ganguly et al., 2004; Moore et al., 2003; Moore & Gibson, 2003; Yamamoto et al. 2006). The initial modulus is used to normalize the applied stress. The following step is the definition of  $(\Delta\sigma/E_0)$  where  $\Delta\sigma$  is the interval of applied stress, *i.e.*,  $\Delta\sigma = \sigma_{\max} - \sigma_{\min}$ . If high values of  $(\Delta\sigma/E_0)$  are imposed it is expected that the material fails at a small number of cycles. The frequency of the cycles varies from 1 to 2 Hz (Dendorfer et al., 2008; Ganguly et al., 2004; Moore et al., 2003; Moore & Gibson, 2003) and values of  $(\Delta\sigma/E_0) = 0.008$  or lower can be used (Moore & Gibson, 2003). It is considered that on a test, failure occurs when the modulus reduction is 10% (Ganguly et al., 2004; Moore et al., 2003; Moore & Gibson, 2003).

From fatigue tests, stress-strain curves are obtained and it is possible to measure the secant modulus (from the slope of each cycle), changes in the plastic strain for a single cycle  $\Delta\varepsilon_{pl}$ , residual strain on unloading  $\varepsilon_{res}$  and maximum strain  $\varepsilon_{\max}$  (Dendorfer et al., 2008; Ganguly et al., 2004; Moore et al., 2003; Moore & Gibson, 2003).

The fatigue behavior of trabecular bone is characterized by an increase on  $\varepsilon_{res}$ , a broadening of the hysteresis loops, and by a decrease of the secant modulus. The strains,  $\varepsilon_{max}$  or  $\varepsilon_{res}$  plotted against the number of cycles, exhibit the typical fatigue curve with three stages. There is an initial increase of the strains with the number of cycles, a zone where the strain rate is almost constant and finally a third zone characterized by a rapid increasing of strains until failure (Dendorfer et al., 2008, Ganguly et al., 2004; Moore et al., 2003; Moore & Gibson, 2003). An example of fatigue curves of trabecular bone from a femoral head of a patient with osteoporosis is given in Figure 14. Figure 14 a) shows the initial preconditioned with 10 cycles, while Figure 14b) presents  $\sigma/E_0$  versus the strain  $\varepsilon$  in a test with 1000 cycles. The modulus  $E_0$  is calculated from the slope of the 10<sup>th</sup> cycle. The ratio of  $(\Delta\sigma/E_0)$  was 0.002. The strains  $\varepsilon_{max}$  or  $\varepsilon_{res}$  increased with the number of cycles. However, the modulus ( $E_{sec}/E_0$ ) was kept almost constant. This is probably due to the application of very small values of stress and a reduced number of cycles.

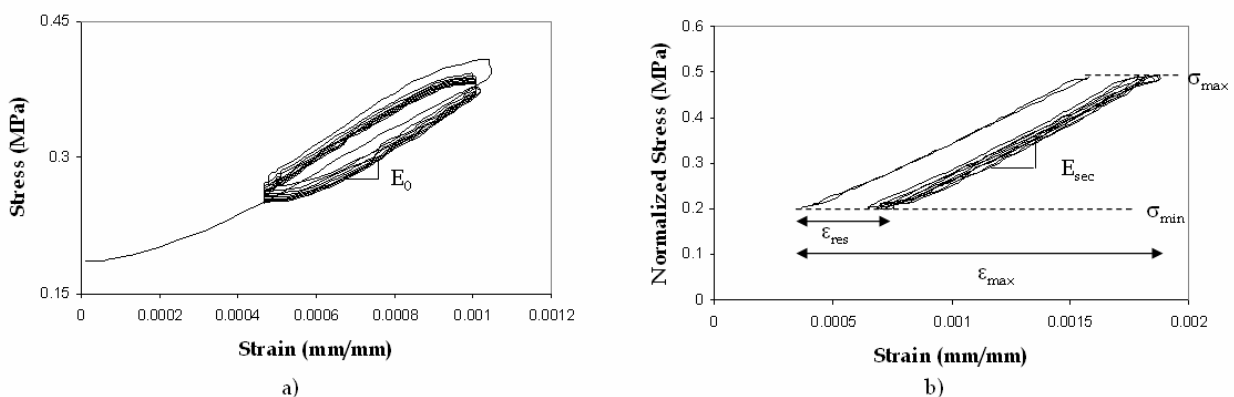


Fig. 14. Fatigue curves of trabecular bone from a femoral head of a patient with osteoporosis: a) initial preconditioned with 10 cycles, b)  $\sigma/E_0$  versus the strain  $\varepsilon$  in a test with 1000 cycles: only cycles n<sup>o</sup> 1, 200, 400, 600, 800 and 1000 are represented

### 3.5 Creep

Like other biological materials, bone exhibits a time-dependent damage or creep (Keaveny et al., 2001). Vertebral fractures present deformations on the vertebrae which indicate a time dependent failure mode, due to irreversible residual strains (Yamamoto et al., 2006). It is suggested that the trabecular bone does not have time to recover from creep deformations accumulated by static loading (Yamamoto et al., 2006).

Creep tests can be made on human vertebral trabecular bone, with cylindrical specimens. Prior to tests, samples were defatted and placed into brass end caps (Yamamoto et al., 2006). First, the samples go through a preconditioned stage, similar to the one performed in fatigue tests, composed by 10 cycles. The initial modulus is recorded. The specimen is then subjected to a static loading for 35h, after which is unloaded for a period of 35h (Yamamoto et al., 2006). Figure 15 presents the strains measured over the loading and unloading stages. Depending on the applied loads, the creep curve may have a different shape from the one of Figure 15, and may exhibit an initial rapid response, a steady state at a constant speed, followed by a rapid increase in deformation before fracture (Keaveny et al., 2001).

Particular attention is given to the residual strains which remain at the end of the unloading phase. Although loads were applied only for 35h, it was found that deformations only

disappear after 1 month (Yamamoto et al., 2006). As vertebrae had no time to recover from prolonged loading, long time effects may contribute to vertebral fractures.

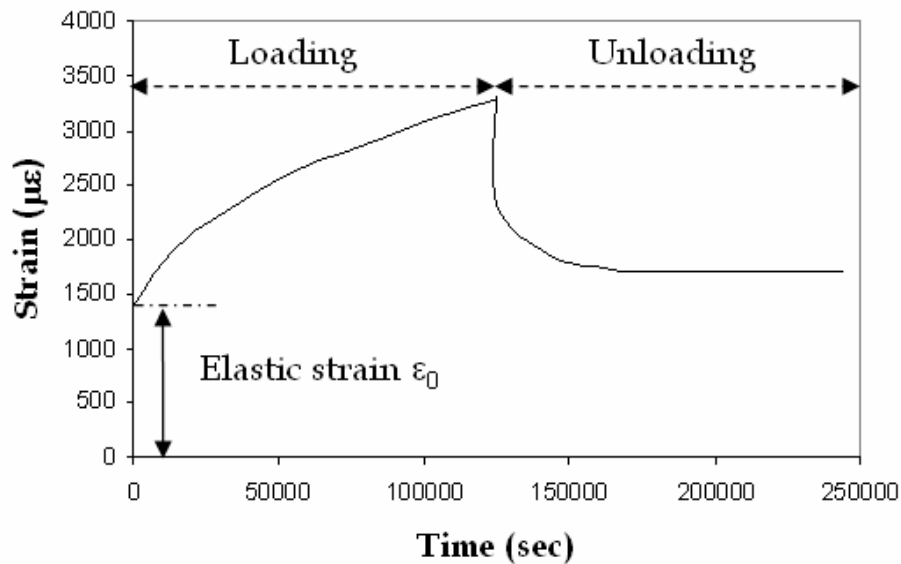


Fig. 15. Typical strain-time curve obtained on a creep test from a vertebral trabecular bone (adapted from (Yamamoto et al., 2006))

### 3.6 Torsion

Bone can be submitted to multiaxial stresses due to bone pathologies, to accidental loads or to a joint replacement (Garnier et al., 1999).

Torsional tests are less frequently used than compression or bending (Sharir et al., 2008). The extremities of the bone sample are embedded in blocks of polymer material which fit the grips of the testing device (Nazarian et al., 2009; Sharir et al., 2008). Deformation rates from 0.01 to 0.36 rad s<sup>-1</sup> may be applied (Kasra & Grynypas, 2007).

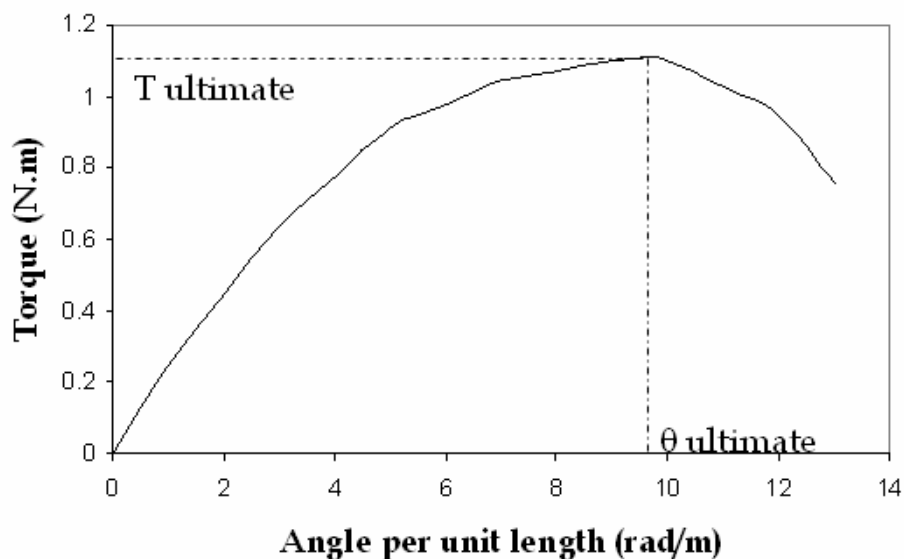


Fig. 16. A typical torque-angular deformation curve from a torsion test with trabecular femoral head bone (adapted from (Garnier et al., 1999))

During a test, the specimen is subjected to a torque that originates its torsion (Sharir et al., 2008). The torque-angular deformation curve is recorded and the shear modulus is calculated from the slope of the linear region (Kasra & Grynypas, 2007; Nazarian et al., 2009; Sharir et al., 2008). The shear stress is also calculated from the data of the torque-angular deformation curve (Garnier et al., 1999). A typical torque deformation curve is shown on Figure 16.

The shear modulus increases with the strain rate, which reveals the viscoelastic nature of the bone tissue (Kasra & Grynypas, 2007). On human femoral trabecular bone, the mean shear modulus was found to be 289 MPa (Garnier et al., 1999), which is similar to the values obtained for animal trabecular bone (Kasra & Grynypas, 2007).

### 3.7 Nanoindentation

Besides structural assessment, AFM can operate to perform nanoindentation, which is used to measure the intrinsic mechanical properties, such as, the bone tissue modulus of trabecular bone (Chevalier et al., 2007) and cortical tissue (Bembey et al., 2006), or the mechanical properties of the bone structural units, *i.e.*, the osteon for cortical bone and the trabeculae wall for trabecular bone (Hengsberger et al., 2001; Rho et al., 1997; Rho et al., 1999; Zysset et al., 1999). Nanoindentation measures the elastic modulus or the stiffness, as well as, the hardness of the bone tissue (Hengsberger et al., 2001).

The combination of AFM and nanoindentation has the possibility of investigating the elastic properties of bone structural units (BSU) associated to a surface characterization, which provides high resolution to the position of the tip on the structure of interest (Hengsberger et al., 2001). The combination of AFM with nanoindentation allows obtaining a surface topography of constant contact force and a force-displacement curve in nanoindentation (Hengsberger et al., 2001).

The procedure to prepare the bone samples includes, besides bone marrow removal by distilled water, and subsequent dehydration, an embedment in a resin and polishing with 1200, 2400 and 4000 grade silicon carbide papers and with alumina suspension (Chevalier et al., 2007; Hengsberger et al., 2001).

Nanoindentation is performed in three phases, which include a loading phase where the tip is pressed into the material up to a maximum force, an holding period where the tip penetrates into the material (Figure 17a)) leaving indentation marks (Figure 17b)) followed by an unloading step. Load-displacement curves are obtained (Figure 17c)). As during loading and holding phases, both elastic and plastic deformation occur, it is only possible to determine the elastic modulus on the unloading phase, where the elastic recovery is the only mechanism present (Hengsberger et al., 2001). The stiffness is determined by the slope of the unloading curve between 40% and 90% of the maximum load (Hengsberger et al., 2001). To determine the contact area the procedure derived by Oliver & Pharr (Oliver & Pharr, 1992) is followed. The hardness is obtained by dividing the maximum load by the contact area (Hengsberger et al., 2001).

The experimental Young's moduli for the bone units vary from 0.76 GPa to 20 GPa for trabecular bone and from 5 GPa to 27 GPa for cortical bone. Hardness presents values of  $0.6 \pm 0.11$  GPa for compact bone and  $1.1 \pm 0.17$  GPa for trabecular bone (Hengsberger et al., 2001).

Other studies propose the combination of AFM with SEM to measure the properties of collagen fibrils (Hang & Barber, 2011) or the combination of AFM with qBEI (Fratzl-Zelman

et al. 2009) to evaluate if a reduced mineral content determined by qBEI is associated with a reduction of the stiffness and hardness of the bone.

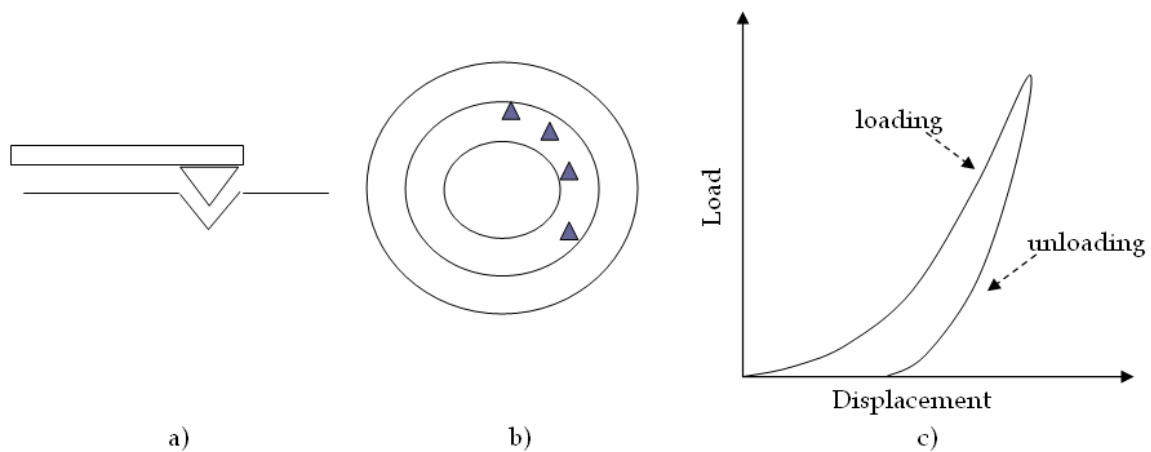


Fig. 17. Schematically nanoindentation a) tip, b) indentation marks on an osteon and c) curve load-displacement (adapted from (Hengsberger et al., 2001))

### 3.8 Bone deformation mechanisms

Several attempts have been made to predict the mechanical properties of bone including the composite rule of mixtures (Rho et al., 1998). As mentioned in Section 2, bone is a composite material formed by mineral crystals of carbonated apatite in a matrix of collagen. As the apatite is a rigid, brittle material, collagen must play an important role on the bone deformation (Fratzl et al., 2004; Fratzl & Weinkamer, 2007). It is assumed that the elastic behavior of bone is dominated by the mineral phase, while the plastic deformation is governed by a combination of the elastic-plastic behavior of the mineral with pure elastic deformation of the collagen matrix (Fratzl et al., 2004; Fratzl & Weinkamer, 2007). The matrix between the mineral particles has the role of dissipating energy, by deviating or creating barriers to crack propagation (Fratzl et al., 2004; Fratzl & Weinkamer, 2007). It has been proposed that the bonds within or between collagen molecules have the ability to recover after load removal, being responsible for the toughness of the bone (Fratzl et al., 2004; Fratzl & Weinkamer, 2007). Bone deformation, for example by tensile loading, induces shear stresses on the matrix, which means that the mechanical performance of bone is controlled by the shear stiffness, strength and toughness of the matrix (Fratzl et al., 2004; Fratzl & Weinkamer, 2007). Following this analysis, within a fibril, the organic matrix should be thin to withstand shear stress and the mineral particles must be thin to reduce the brittleness of the tissue (Fratzl et al., 2004; Fratzl & Weinkamer, 2007). As a result, the mechanical behavior of the bone, as a composite material, depends on its components, collagen and mineral particles and on the interaction between them.

### 3.9 The effect of aging and disease on the bone's mechanical properties

There is some uncertainty in the prediction of mechanical behavior of bone influenced by aging or bone disease.

Aging, is associated with changes in bone structure and microarchitecture, decreased bone strength and increased the risk of fragility fractures, due to a decrease in bone volume formed, continued resorption and high remodeling (Seeman, 2007, 2008). In post menopause

women, increased remodeling induces cortical thinning, higher porosity, trabecular thinning as well as loss of trabeculae connectivity (Seeman, 2007, 2008). High remodeling also decreases the bone mineral content, which is reflected on a reduction of stiffness (Seeman, 2007).

It was found that with aging, a significant loss on the mechanical strength is observed, as the yield stress is reduced by 10% per decade, from the 2<sup>nd</sup> decade to the 10<sup>th</sup> decade (Keaveny et al., 2001).

### 3.9.1 Metabolic bone diseases

There are some studies on the effect of osteoporosis on the mechanical properties of bone (Ciarelli et al., 2000; Homminga et al. 2002; Sun et al., 2008; Woo et al., 2010). Osteoporotic individuals have worse mechanical properties, evaluated by the Young's modulus and yield stress, in comparison with controls (Ciarelli et al., 2000). Differences were also detected in the other methods performed.

### 3.9.2 Inflammatory rheumatic diseases

The effect of arthritis in the mechanical deformation either in compression and bending were previously described in sections 3.1 and 3.3, for SKG mice (Caetano-Lopes et al., 2009a). In fact, arthritic mice vertebrae were found to have lower stiffness, strength and toughness in comparison with the results obtained on the compression of control BALB/c mice (Caetano-Lopes et al., 2009a, 2010). Moreover we have also observed in these mice degradation of mechanical properties studied by femur bending tests.

Compression tests performed on human osteoporotic samples and on osteoarthritis samples revealed that specimens with osteoporosis had lower Young's modulus and yield stress than the ones with osteoarthritis (Li & Aspden, 1997; Sun et al., 2008).

## 4. Conclusions

This chapter gave a general approach of the bone as a composite material with particular emphasis on the bone structural and mechanical properties. Essentially the line followed was to focus on the experimental procedures and on the techniques used for bone assessment. Some aspects were not covered as the finite element modeling, which the authors considered to be out of the scope of the chapter. Results from research studies performed by the authors, namely in a mice model of arthritis and in human bone samples obtained from patients submitted to total hip replacement surgery were presented to illustrate the impact of the inflammation on bone and also whether the bone mechanical and structural properties can be affected in primary and secondary osteoporosis.

## 5. References

- Akhter, M.; Cullen, D.; Gong, G. & Recker, R. (2001). Bone biomechanical properties in Prostaglandin EP1 and EP2 knockout mice. *Bone*, Vol. 29, pp.121-125, ISSN 8756-3282.
- Alamanos, Y. & Drosos, A. (2005). Epidemiology of adult rheumatoid arthritis. *Autoimmunity Reviews*, Vol.4, No.3, pp. 130-136, ISSN 1568-9972.

- Ammann, P. & Rizzoli, R. (2003). Bone strength and its determinants. *Osteoporosis International*, Vol.14, pp. S13-S18, ISSN 0937-941X.
- Basillais, A.; Bensamoun, S.; Chappard, C.; Brunet-Imbault, B.; Lemineur, G.; Ilharreborde, B.; Ho Ba Tho, M. & Benhamou, C. (2007). Three-dimensional characterization of cortical bone microstructure by microcomputed tomography: validation with ultrasonic and microscopic measurements. *Journal of Orthopaedic Science*, Vol.12, No.2, pp. 141-148, ISSN 0949-2658.
- Bayraktar, H.; Morgan, E.; Niebur, G.; Morris, G.; Wong, E. & Keaveny, T. (2004). Comparison of the elastic and yield properties of human femoral trabecular and cortical bone tissue. *Journal of Biomechanics*, Vol.37, No.1, pp. 27-35, ISSN 0021-9290.
- Beer, F.; Johnston, E. & DeWolf, J. (1992). *Mechanics of Materials* (2<sup>nd</sup> Ed.). McGraw-Hill, ISBN0-070-04340-X, New York, USA.
- Bembey, A.; Bushby, A.; Boyde, A.; Ferguson, V. & Oyen, M. (2006). Hydration effects on the micro-mechanical properties of bone. *Journal of Materials Research*, Vol.21, No.8, pp. 1962-1968, ISSN 0884-2914.
- Bensamoun, S.; Subramaniam, M.; Hawse, J.; Ilharreborde, B.; Bassillais, A.; Benhamou, C.; Fraser, D.; Oursler, M.; Amadio, P.; Na, K. & Spelsberg, T. (2006). TGF- $\beta$  inducible early gene-1 knockout mice display defects in bone strength and microarchitecture. *Bone*, Vol.39, No.6, pp. 1244-1251, ISSN 8756-3282.
- Bevill, G.; Farhamand, F. & Keaveny, T. (2009). Heterogeneity of yield strain in low-density versus high-density human trabecular bone. *Journal of Biomechanics*, Vol.42, No.13, pp. 2165-2170, ISSN 0021-9290.
- Bonewald, L. (2011). The amazing osteocyte. *Journal of Bone and Mineral Research*, Vol. 26, pp. 229-238, ISSN 1523-4681.
- Boyde, A; Bianco, P.; Barbos, M. & Ascenzi, A. (1984). Collagen orientation in compact-bone. A new method for the determination of the proportion of collagen parallel to the plane of compact-bone sections. *Metabolic Bone Disease and Related Research*, Vol.6, No.6, pp. 299-307, ISSN 0221-8747.
- Boyle, W.; Simonet, W. & Lacey, D. (2003). Osteoclast differentiation and activation. *Nature*, Vol.423, pp. 337-342, ISSN 0028-0836.
- Bozec, L.; de Groot, J.; Odlyha, M.; Nicholls, B. & Horton, M. (2005). Mineralised tissues as nanomaterials: Analysis by atomic force microscopy. *IEE Proceedings Nanobiotechnology*, Vol.152, No.5, pp.183-186, ISSN 1478-1581.
- Buehler, M. (2006). Nature design tough collagen: explaining the nanostructure of collagen fibrils. *Proceedings of the National Academy of Sciences of the United States of America*, Vol.103, No.33, pp.12285-12290.
- Buehler, M. (2007). Molecular nanomechanics of nascent bone: fibrillar toughening by mineralization. *Nanotechnology*, Vol.18, No.29, pp. 295102, ISSN 0957-4484.
- Bunger, M.; Oxlund, H.; Hansen, T.; Sørensen, S.; Bibby, B.; Thomsen, J.; Langdahl, B.; Besenbacher, B; Pedersen, J. & Birkedal, H. (2010). Strontium and Bone Nanostructure in Normal and Ovariectomized Rats Investigated by Scanning Small-Angle X-Ray Scattering. *Calcified Tissue International*, Vol.86, No.4, pp.294-306, ISSN 0171-967X.
- Caetano-Lopes, J.; Nery, A.; Henriques, R.; Canhão, H.; Duarte, J.; Amaral, P.; Vale, M.; Moura, R.; Pereira, P.; Weinmann, P.; Abdulghani, S.; Souto-Carneiro, M.; Rego, P.; Monteiro, J.; Sakagushi, S.; Konttinen, Y.; Graça, L.; Queiroz, M.; Vaz, M. &

- Fonseca, J. (2009a). Chronic arthritis directly induces quantitative and qualitative bone disturbances leading to compromised biomechanical properties. *Clinical and Experimental Rheumatology*, Vol.27, No.3, pp.475-482, ISSN 0392-856X.
- Caetano-Lopes, J; Canhão, H. & Fonseca, J. (2009b). Osteoimmunology - The hidden immune regulation of bone. *Autoimmunity Reviews*, Vol.8, No.3, pp. 250-255, ISSN 1568-9972.
- Caetano-Lopes, J.; Nery, A.; Canhão, H.; Duarte, J.; Cascão, R.; Rodrigues, A.; Perpétuo, I.; Abdulghani, S.; Amaral, P.; Sakaguchi, S.; Konttinen, Y.; Graça, L.; Vaz, M. & Fonseca, J. (2010). Chronic arthritis leads to disturbances in the bone collagen network. *Arthritis Research & Therapy*, Vol.12, R9, ISSN 1478-6362.
- Chappard, C.; Marchadier, A. & Benhamou, L. (2008). Interindividual and intraspecimen variability of 3-D bone microarchitectural parameters in iliac crest biopsies imaged by conventional micro-computed tomography. *Journal of Bone and Mineral Metabolism*, Vol.26, No.5, pp. 506-513, ISSN 0914-8779.
- Chevalier, Y.; Pahr, D.; Allmer, H.; Charlebois, M. & Zysset, P. (2007). Validation of a voxel-based FE method for prediction of the uniaxial apparent modulus of human trabecular bone using macroscopic mechanical tests and nanoindentation. *Journal of Biomechanics*, Vol.40, No.15, pp. 3333-3340, ISSN 0021-9290.
- Ciarallo, A.; Barralet, J.; Tanzer, M. & Kremer, R. (2006). An approach to compare the quality of cancellous bone from the femoral necks of healthy and osteoporotic patients through compression testing and microcomputed tomography imaging. *McGrill Journal of Medicine*, Vol.9, No.2, pp. 102-107, ISSN 1201-026X.
- Ciarelli, T.; Fyhrie, D.; Schaffler, M. & Goldstein, S. (2000). Variations in Three-Dimensional Cancellous Bone Architecture of the Proximal Femur in Female Hip Fractures and in Controls. *Journal of Bone and Mineral Research*, Vol.15, No.1, pp. 32-40, ISSN 0884-0431.
- Cooper, D.; Turinsky, A.; Sensen, C. & Hallgrímsson, B. (2007a). Effect of voxel size on 3D micro-CT analysis of cortical bone porosity. *Calcified Tissue International*, Vol.80, No.3, pp. 211-219, ISSN 0171-967X.
- Cooper, D.; Thomas, C.; Clement, J.; Turinsky, A.; Sensen, C. & Hallgrímsson, B. (2007b). Age-dependent change in the 3D structure of cortical porosity at the human femoral midshaft. *Bone*, Vol.40, No.4, pp. 957-965, ISSN 8756-3282.
- Cory, E.; Nazarian, A.; Entezari, V.; Vartanians, V.; Muller, R. & Snyder, B. (2010). Compressive axial mechanical properties of rat bone as functions of bone volume fraction, apparent density and micro-CT based mineral density. *Journal of Biomechanics*, Vol.43, No.5, pp. 953-960, ISSN 0021-9290.
- Cox, G. & Kable, E. (2006). Second-harmonic imaging of collagen. *Methods in Molecular Biology*, Vol.319, pp.15-35, ISSN 1064-3745.
- Cox, G.; Kable, E.; Jones, A.; Fraser, I.; Manconi, F. & Gorrell, M. (2003). 3-dimensional imaging of collagen using second harmonic generation. *Journal of Structural Biology*, Vol.141, No.1, pp. 53-62, ISSN 1047-8477.
- Cowin, S. (2001). *Bone mechanics handbook* (2<sup>nd</sup> Ed.), CRC Press, ISBN 0-8493-9117-2, Boca Raton, USA.
- Dendorfer, S.; Maier, H.; Taylor, D. & Hammer J. (2008). Anisotropy of the fatigue behaviour of cancellous bone. *Journal of Biomechanics*, Vol.41, No.3, pp. 636-641, ISSN 0021-9290.

- Dendorfer, S.; Maier, H. & Hammer, J. (2009). Fatigue damage in cancellous bone: An experimental approach from continuum to micro scale. *Journal of the Mechanical Behavior of Biomedical Materials*, Vol. 2, No. 1, ISSN 1751-6161.
- Diamant, I.; Shahar, R.; Masharawi, Y. & Gefen, A. (2007). A method for patient-specific evaluation of vertebral cancellous bone strength: In vitro validation. *Clinical Biomechanics*, Vol.22, No.3, pp. 282-291, ISSN 0268-0033.
- Diederichs, G.; Link, T.; Kentenich, M.; Schwieger, K.; Huber, M.; Burghardt, A.; Majumdar, S.; Rogalla, P. & Issever, A. (2009). Assessment of trabecular bone structure of the calcaneus using multi-detector CT: Correlation with microCT and biomechanical testing. *Bone*, Vol.44, No.5, pp. 976-983, ISSN 8756-3282.
- Ding, M.; Odgaard, A. & Hvid, I. (1999). Accuracy of cancellous bone volume fraction measured by micro-CT scanning. *Journal of Biomechanics*, Vol.32, No. 3, pp. 323-326, ISSN 0021-9290.
- Djuric, M.; Djonic, D.; Milovanovic, P.; Nikolic, S.; Marshall, R.; Marinkovic, J. & Hahn, M. (2010). Region-Specific Sex-Dependent Pattern of Age-Related Changes of Proximal Femoral Cancellous Bone and Its Implications on Differential Bone Fragility. *Calcified Tissue International*, Vol.86, No.3, pp. 192-201, ISSN 0171-967X.
- Duan, Y.; Wang, X.-F.; Evans, A. & Seeman, E. (2005). Structural and biomechanical basis of racial and sex differences in vertebral fragility in Chinese and Caucasians. *Bone*, Vol.36, No.6, pp. 987-998, ISSN 8756-3282.
- Fantner, G.; Birkedal, H.; Kindt, J.; Hassenkam, T.; Weaver, J.; Cutroni, J.; Bosma, B.; Bawazer, L.; Finch, M.; Cidade, G.; Morse, D.; Stucky, G. & Hansma, P. (2004). Influence of the degradation of the organic matrix on the microscopic fracture behavior of trabecular bone. *Bone*, Vol.35, No.5, pp. 1013-1022, ISSN 8756-3282.
- Fonseca, D. & Ward, W. (2004). Daidzein together with high calcium preserve bone mass and biomechanical strength at multiple sites in ovariectomized mice. *Bone*, Vol.35, No.2, pp. 489-497, ISSN 8756-3282.
- Fratzl, P.; Gupta, H.; Paschalis, E. & Roschger, P. (2004). Structure and mechanical quality of the collagen-mineral nano-composite in bone. *Journal of Materials Chemistry*, Vol.14, No.14, pp. 2115-2123, ISSN 0959-9428.
- Fratzl, P. & Weinkamer, R. (2007). Nature's hierarchical materials. *Progress in Materials Science*, Vol.52, No.8, pp. 1263-1334, ISSN 0079-6425.
- Fratzl-Zelman, N.; Roschger, P.; Gourrier, A.; Weber, M.; Misof, B.; Loveridge, N.; Reeve, J.; Klaushofer, K. & Fratzl, L. (2009). Combination of nanoindentation and quantitative backscattered electron imaging revealed altered bone material properties associated with femoral neck fragility. *Calcified Tissue International*, Vol.85, No.4, pp. 335-343, ISSN 0171-967X.
- Fung, Y. (1993). *Biomechanics: mechanical properties of living tissues* (2<sup>nd</sup> Ed.), Springer Verlag, ISBN 0-387-97947-6, New York, USA.
- Ganguly, P.; Moore, T.; Gibson, L. (2004). A Phenomenological Model for Predicting Fatigue Life in Bovine Trabecular Bone. *Journal of Biomechanical Engineering*, Vol.126, No.3, pp. 330-339, ISSN 0148-0731.
- Garnier, K.; Dumas, R.; Rumelhart, C. & Arlot, M. (1999). Mechanical characterization in shear of human femoral cancellous bone: torsion and shear tests. *Medical Engineering & Physics*, Vol.21, No.9, pp. 641-649, ISSN 1350-4533.

- Gibson, L. & Ashby, M. (1999). *Cellular Solids, Structure and Properties* (2<sup>nd</sup> Ed.), Cambridge University Press, ISBN 0-5214-9911-9, Cambridge, UK.
- Gibson, L. (2005). Biomechanics of cellular solids. *Journal of Biomechanics*, Vol.38, No.3, pp. 377-399, ISSN 0021-9290.
- Giraud-Guille, M. (1988). Twisted plywood architecture of collagen fibrils in human compact bone osteons. *Calcified Tissue International*, Vol.42, No.3, pp. 167-180, ISSN 0171-967X.
- Goodhew, P. & Humphreys, F. (2000). *Electron Microscopy and Analysis* (3<sup>rd</sup> Ed.). Taylor and Francis, ISBN 0-748-40968-8, London, UK.
- Haddock, S.; Yeh, O.; Mummaneni, P.; Rosenberg, W. & Keaveny, T. (2004). Similarity in the fatigue behaviour of trabecular bone across site and species. *Journal of Biomechanics*, Vol.37, No.2, pp. 181-187, ISSN 0021-9290.
- Hang, F. & Barber, A. (2011). Nano-mechanical properties of individual mineralized collagen fibrils from bone tissue. *Journal of the Royal Society Interface*, Vol.8, No.57, pp. 500-505, ISSN 1742-5689.
- Hassenkam, T.; Fantner, G.; Cutroni, J.; Weaver, J.; Morse, D. & Hansma, P. (2004). High-resolution AFM imaging of intact and fractured trabecular bone. *Bone*, Vol.35, No.1, pp. 4-10, ISSN 8756-3282.
- Hassenkam, T.; Jorgensen, H. & Lauritzen, J. (2006). Mapping the imprint of bone remodelling by atomic force microscopy. *The Anatomical Record. Part A, Discoveries in Molecular, Cellular and Evolutionary Biology*, Vol.288A, No.10, pp.1087-1094, ISSN 1552-4884.
- Helgason, B.; Perilli, E.; Schileo, E. & Taddei, F. (2008). Mathematical relationships between bone density and mechanical properties: A literature review. *Clinical Biomechanics*, Vol.23, No.2, pp. 135-146, ISSN 0268-0033.
- Hengsberger, S.; Kulik, A. & Zysset, P. (2001). A combined atomic force microscopy and nanoindentation technique to investigate the elastic properties of bone structural units. *European Cells & Materials*, Vol.1, pp. 12-17, ISSN 1473-2262.
- Homminga, J.; McCreadie, B.; Ciarelli, T.; Weinans, H.; Goldstein, S. & Huiskes, R. (2002). Cancellous Bone Mechanical Properties from Normals and Patients with Hip Fractures Differ on the Structure level not on the Bone Hard Tissue Level. *Bone*, Vol.30, No.5, pp. 759-764, ISSN 8756-3282.
- Hull, D. (1981). *An introduction to composite materials* (1<sup>st</sup> Ed.), Cambridge University Press, ISBN 0-521-38190-8, Cambridge, UK.
- Jiang, Y.; Zhao, J.; Mitlak, B.; Wang, O.; Genant, H. & Eriksen, E. (2003). Recombinant Human Parathyroid Hormone (1-34) [Teriparatide] Improves Both Cortical and Cancellous Bone Structure. *Journal of Bone and Mineral Research*, Vol.18, No.11, pp. 1932-1941, ISSN 0884-0431.
- Kanis, J.; Cooper, C.; Burlet, N.; Delmas, P.; Reginster, J.-Y.; Borgstrom, F. & Rizzoli, R. (2005). European guidance for the diagnosis and management of osteoporosis in post menopausal women, Available from: <<http://www.shef.ac.uk/FRAX>>.
- Kasra, M. & Grynpas, M. (2007). On the shear properties of trabecular bone under torsional loading: effects of bone marrow and strain rate. *Journal of Biomechanics*, Vol.40, No.13, pp. 2898-2903, ISSN 0021-9290.
- Keaveny, T.; Morgan, E.; Niebur, G. & Yeh, O. (2001). Biomechanics of Trabecular Bone. *Annual Review of Biomedical Engineering*, Vol.3, pp. 307-333, ISSN 1523-9829.

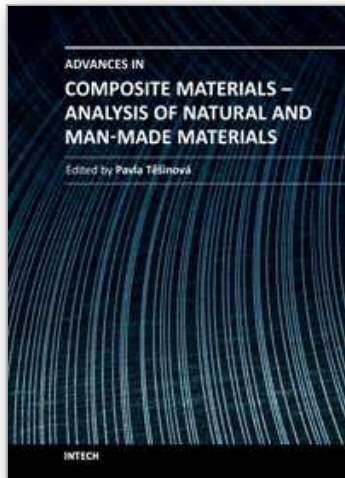
- Knoob, T.; Pringle, D.; Gedbaw, E.; Meredith, J.; Berrios, R. & Kim, H. (2007). Biomechanical properties of bone and cartilage in growing femoral heads following ischemic osteonecrosis. *Journal of Orthopaedic Research*, Vol.25, No.6, pp. 750-757, ISSN 0736-0266.
- Kopperdahl, D. & Keaveny, T. (1998). Yield strain behavior of trabecular bone. *Journal of Biomechanics*, Vol.31, No.7, pp. 601-608, ISSN 0021-9290.
- Lakes, R. (2003). Composite Biomaterials, In: *Biomaterials: Principles and Applications*, J. B. Park & J. D. Bronzino, (Ed.), CRC Press, ISBN 0-849-31491-7, Boca Raton, USA.
- Li, B. & Aspden, R. (1997). Composition and mechanical properties of cancellous bone from the femoral head of patients with osteoporosis or osteoarthritis. *Journal of Bone and Mineral Research*, Vol.12, No.4, pp. 641-651, ISSN 0884-0431.
- Link, T.; Majumdar, S.; Lin, J.; Augat, P.; Gould, R.; Newitt, D.; Ouyang, X.; Lang, T.; Mathur, A. & Genant, H. (1998). Assessment of trabecular structure using high resolution CT images and texture analysis. *Journal of Computer Assisted Tomography*, Vol.22, No.1, pp. 15-24, ISSN 0363-8715.
- Macho, G.; Abel, R. & Schutkowski, H. (2005). Age Changes in Bone Microstructure: Do They Occur Uniformly? *International Journal of Osteoarchaeology*, Vol.15, No.6, pp. 421-430, ISSN 1047-482X.
- Matsuura, M.; Eckstein, F.; Lochmuller, E. & Zysset, P. (2008). The role of fabric in the quasi-static compressive mechanical properties of human trabecular bone from various anatomical locations. *Biomechanics and Modeling in Mechanobiology*, Vol.7, No.1, pp. 27-42, ISSN 1617-7959.
- Moore, T. & Gibson, L. (2003). Fatigue Microdamage in Bovine Trabecular Bone. *Journal of Biomechanical Engineering*, Vol.125, No.6, pp. 769-776, ISSN 0148-0731.
- Moore, T. & Gibson, L. (2003). Fatigue in Bovine Trabecular Bone. *Journal of Biomechanical Engineering*, Vol.125, No.6, pp. 761-768, ISSN 0148-0731.
- Morgan, E. & Keaveny, T. (2001). Dependence of yield strain of human trabecular bone on anatomic site. *Journal of Biomechanics*, Vol.34, No.5, pp. 569-577, ISSN 0021-9290.
- Morgan, E.; Bayraktar, H. & Keaveny, T. (2003). Trabecular bone modulus-density relationships depend on anatomic site. *Journal of Biomechanics*, Vol.36, No.7, pp. 897-904, ISSN 0021-9290.
- Mueller, T.; van Lenthe, G.; Stauber, M. & Gratzke, C. (2009). Regional, age and gender differences in architectural measures of bone quality and their correlation to bone mechanical competence in the human radius of an elderly population. *Bone*, Vol.45, No.5, pp. 882-891, ISSN 8756-3282.
- Nazarian, A.; Muller, J.; Zurakowski, D.; Muller, R. & Snyder, B. (2007). Densitometric, morphometric and mechanical distributions in the human proximal femur. *Journal of Biomechanics*, Vol.40, No.11, pp. 2573-2579, ISSN 0021-9290.
- Nazarian, A.; Meier, D.; Muller, R. & Snyder, B. (2009). Functional dependence of cancellous bone shear properties on trabecular microstructure evaluated using time-lapsed micro-computed tomographic imaging and torsion testing. *Journal of Orthopaedic Research*, Vol.27, No.12, pp. 1667-1674, ISSN 0736-0266.
- Nicolella, D.; Ni, Q. & Chan, K. (2011). Non-destructive characterization of microdamage in cortical bone using low field pulsed NMR. *Journal of the Mechanical Behavior of Biomedical Materials*, Vol.4, No.3, pp.383-391, ISSN 1751-6161.

- Oliver, W. & Pharr, G. (1992). An improved technique for determining hardness and elastic modulus using load and displacement sensing indentation experiments. *Journal of Materials Research*, Vol.7, No.6, pp. 1564-1583, ISSN 0884-2914.
- Orstavik, R.; Haugeberg, G.; Mowinckel, P.; Hoiseth, A.; Uhlig, T.; Falch, J.; Halse, J.; McColskey, E. & Kvien, T. (2004). Vertebral deformities in rheumatoid arthritis: a comparison with population-based controls. *Archives of Internal Medicine*, Vol.164, No.4, pp. 420-425, ISSN 0003-9926.
- Parfitt, A.; Drezner, M.; Glorieux, F.; Kanis, J.; Malluche, H.; Meunier, P.; Ott, S. & Recker, R. (1987). Bone histomorphometry: standardization of nomenclature, symbols, and units. *Journal of Bone and Mineral Research*, Vol.2, No.6, pp. 595-610, ISSN 0884-0431.
- Park, J. & Lakes, R. (1992). *Biomaterials: an introduction* (2<sup>nd</sup> Ed.), Plenum Press, ISBN 0-306-43992-1, New York, USA.
- Pereira, M.; Mauricio, A.; Vale, A.; Vidal, B.; Rodrigues, A.; Caetano-Lopes, J.; Fonseca, J. E.; Canhão, H.; Vaz, M.F.; paper in preparation
- Ramasamy, J. & O. Akkus, O. (2007). Local variations in the micromechanical properties of mice femur: the involvement of collagen fibre orientation and mineralization. *Journal of Biomechanics*, Vol.40, No.4, pp. 910-918, ISSN 0021-9290.
- Rapillard, L.; Charlebois, M & Zysset, P. (2006). Compression fatigue behavior of human vertebral trabecular bone. *Journal of Biomechanics*, Vol.39, No.11, pp. 2133-2139, ISSN 0021-9290.
- Rho, J.; Tsui, Y. & Pharr, G. (1997). Elastic properties of human cortical and trabecular lamellar bone measured by nanoindentation. *Biomaterials*, Vol.18, No.20, pp. 1325-1330, ISSN 0142-9612.
- Rho, J.; Kuhn-Spearing, L. & Zioupos, P. (1998). Mechanical properties and the hierarchical structure of bone. *Medical Engineering & Physics*, Vol.20, No.2, pp. 92-102, ISSN 1350-4533.
- Rho, J.; Roy, M.; Tsui, T. & Pharr, G. (1999). Elastic properties of microstructural components of human bone tissue as measured by nanoindentation. *Journal of Biomedical Materials Research*, Vol.45, No.1, pp. 48-54, ISSN 0021-9304.
- Roschger, P.; Fratzl, P.; Eschberger, J. & Klaushofer, K. (1998). Validation of Quantitative Backscattered Electron Imaging for the Measurement of Mineral Density Distribution in Human Bone Biopsies. *Bone*, Vol.23, No.4, pp.11-20, ISSN 8756-3282.
- Roschger, P.; Paschalis, E.; Fratzl, P. & Klaushofer, K. (2008). Bone mineralization density distribution in health and disease. *Bone*, Vol.42, No.3, pp.456-466, ISSN 8756-3282.
- Roschger, P.; Lombardi, A.; Misof, B.; Maier, G.; Fratzl-Zelman, N.; P Fratzl, P. & Klaushofer, K. (2010). Mineralization Density Distribution of Postmenopausal Osteoporotic Bone Is Restored to Normal After Long-Term Alendronate Treatment: qBEI and sSAXS Data From the Fracture Intervention Trial Long-Term Extension (FLEX). *Journal of Bone and Mineral Research*, Vol.25, No.1, pp. 48-55, ISSN 0884-0431.
- Rubin, M.; Rubin, J. & Jasiuk, I. (2004). SEM and TEM study of the hierarchical structure of C57BL/6J and C3H/HeJ mice trabecular bone. *Bone*, Vol.35, No.1, pp.11-20, ISSN 8756-3282.
- Schriefer, J.; Robling, A.; Warden, S.; Fournier, A.; Mason, J. & Turner, C. (2005). A comparison of mechanical properties derived from multiple skeletal sites in mice. *Journal of Biomechanics*, Vol.38, No.3, pp. 467-475, ISSN 0021-9290.

- Seeman, E. (2003). The structural and biomechanical basis of the gain and loss of bone strength in women and men. *Endocrinology and Metabolism Clinics of North America*, Vol. 32, No.1, pp. 25-38, ISSN 0889-8529.
- Seeman, E. (2007). Bone's material and structural strength. *Journal of Bone and Mineral Metabolism*, Vol.26, No.1, pp. 1-8, ISSN 0914-8779.
- Seeman, E. (2008). Structural basis of growth-related gain and age-related loss of bone strength. *Rheumatology*, Vol.47, No.4, pp. iv2-iv8, ISSN 1462-0324.
- Shahnazari, M.; Lang, D.; Fosmire, G.; Sharkey, N.; Mitchell, A. & Leach, R. (2007). Strontium administration in young chickens improves bone volume and architecture but does not enhance bone structural and material strength. *Calcified Tissue International*, Vol.80, No.3, pp.160-166, ISSN 0171-967X.
- Sharir, A.; Barak, M. & Shahar, R. (2008). Whole bone mechanics and mechanical testing. *Veterinary Journal*, Vol.177, No.1, pp. 8-17, ISSN 1090-0233.
- Silva, M. (2007). Biomechanics of osteoporotic fractures. *Injury*, Vol.38, No.3, pp. 69-76, ISSN 0020-1383.
- Sun, S.-S.; Ma, H.-L.; Liu, C.-L.; Huang, C.-H.; Cheng, C.-K. & Wei, H.-W. (2008). Difference in femoral head and neck material properties between osteoarthritis and osteoporosis. *Clinical Biomechanics*, Vol.23, pp. S39-S47, ISSN 0268-0033.
- Taylor, D. (1998). Fatigue of Bone and Bones: An Analysis Based on Stressed Volume. *Journal of Orthopaedic Research*, Vol.16, No.2, pp.163-169, ISSN 0736-0266.
- Teo, J.; Teo, E.; Shim, V. & Teoh, S. (2006). Determination of Bone Trabeculae Modulus – An Ultrasonic Scanning and MicroCT ( $\mu$ CT) Imaging Combination Approach, *Experimental Mechanics*, Vol.46, No.4, pp. 453-461, ISSN 0014-4851.
- Teo, J.; Si-Hoe, K.; Keh, J. & Teoh, S. (2007). Correlation of cancellous bone microarchitectural parameters from microCT to CT number and bone mechanical properties. *Materials Science & Engineering*, Vol.27, No.2, pp. 333-339, ISSN 0928-4931.
- Vale, A.C.; Aleixo, I.P.; Lúcio, M.; Saraiva, A.; Caetano-Lopes, J.; Rodrigues, A.; Amaral, P. M.; Rosa, L. G.; Monteiro, J.; Fonseca, J. E.; Vaz, M. F.; Canhão, H.; paper in preparation.
- van Staa, T.; Geusens, P.; Bijlsma, J.; Leufkens, H. & Cooper, C. (2006). Clinical assessment of the long-term risk of fracture in patients with rheumatoid arthritis. *Arthritis and Rheumatism*, Vol.54, No.10, pp. 3104-3112, ISSN 0004-3591.
- Viguet-Carrin, S.; Garnero, P. & Delmas, P. (2006). The role of collagen in bone strength. *Osteoporosis International*, Vol.17, No.3, pp. 319-336, ISSN 0937-941X.
- Wachter, N.; Augat, P.; Krischak, G.; Mentzel, M.; Kinzl, L. & Claes, L. (2001). Prediction of cortical bone porosity in vitro by microcomputed tomography. *Calcified Tissue International*, Vol.68, No.1, pp. 38-42, ISSN 0171-967X.
- Wang, X.; Shen, X.; Li, X. & Agrawal, C. (2002). Age-related Changes in the Collagen Network and Toughness of Bone. *Bone*, Vol.31, No.1, pp. 1-7, ISSN 8756-3282.
- Wang, X.-F.; Duan, Y.; Beck, T. & Seeman, E. (2005). Varying contributions of growth and ageing to racial and sex differences in femoral neck structure and strength in old age. *Bone*, Vol.36, No.6, pp. 978-986, ISSN 8756-3282.
- Weiner, S. & Traub, W. (1992). Bone-structure - from angstroms to microns. *Journal of the Federation of American Societies for Experimental Biology*, Vol.6, pp. 879-885, ISSN 0892-6638.

- Weiner, S. & Wagner, H. (1998). The material bone: structure mechanical function relations. *Annual Review of Materials Science*, Vol.28, No.1, pp. 271-298, ISSN 0084-6600.
- Weiner, S.; Traub, W. & Wagner, H. (1999). Lamellar Bone: Structure-Function Relations. *Journal of Structural Biology*, Vol.126, No.3, pp. 241-255; ISSN 1047-8477.
- Woo, D.; Kim, C.; Lim, D. & Kim, H. (2010). Experimental and simulated studies on the plastic mechanical characteristics of osteoporotic vertebral trabecular bone. *Current Applied Physics*, Vol.28, No.3, pp. 729-733, ISSN 1567-1739.
- Yamamoto, E.; Crawford, R.; Chan, D. & Keaveny, T. (2006). Development of residual strains in human vertebral trabecular bone after prolonged static and cyclic loading at low load levels. *Journal of Biomechanics*, Vol.39, No.10, pp. 1812-1818, ISSN 0021-9290.
- Zysset, P.; Guo, X.; Hoffler, C.; Moore, K. & Goldstein, S. (1999). Elastic modulus and hardness of cortical and trabecular bone lamellae measured by nanoindentation in the human femur. *Journal of Biomechanics*, Vol.32, No.10, pp. 1005-1012, ISSN 0021-9290.

IntechOpen



## **Advances in Composite Materials - Analysis of Natural and Man-Made Materials**

Edited by Dr. Pavla Tesinova

ISBN 978-953-307-449-8

Hard cover, 572 pages

**Publisher** InTech

**Published online** 09, September, 2011

**Published in print edition** September, 2011

Composites are made up of constituent materials with high engineering potential. This potential is wide as wide is the variation of materials and structure constructions when new updates are invented every day.

Technological advances in composite field are included in the equipment surrounding us daily; our lives are becoming safer, hand in hand with economical and ecological advantages. This book collects original studies concerning composite materials, their properties and testing from various points of view. Chapters are divided into groups according to their main aim. Material properties are described in innovative way either for standard components as glass, epoxy, carbon, etc. or biomaterials and natural sources materials as ramie, bone, wood, etc. Manufacturing processes are represented by moulding methods; lamination process includes monitoring during process. Innovative testing procedures are described in electrochemistry, pulse velocity, fracture toughness in macro-micro mechanical behaviour and more.

### **How to reference**

In order to correctly reference this scholarly work, feel free to copy and paste the following:

Maria Fátima Vaz, Helena Canhão and João Eurico Fonseca (2011). Bone: A Composite Natural Material, *Advances in Composite Materials - Analysis of Natural and Man-Made Materials*, Dr. Pavla Tesinova (Ed.), ISBN: 978-953-307-449-8, InTech, Available from: <http://www.intechopen.com/books/advances-in-composite-materials-analysis-of-natural-and-man-made-materials/bone-a-composite-natural-material>

**INTECH**  
open science | open minds

### **InTech Europe**

University Campus STeP Ri  
Slavka Krautzeka 83/A  
51000 Rijeka, Croatia  
Phone: +385 (51) 770 447  
Fax: +385 (51) 686 166  
[www.intechopen.com](http://www.intechopen.com)

### **InTech China**

Unit 405, Office Block, Hotel Equatorial Shanghai  
No.65, Yan An Road (West), Shanghai, 200040, China  
中国上海市延安西路65号上海国际贵都大饭店办公楼405单元  
Phone: +86-21-62489820  
Fax: +86-21-62489821

© 2011 The Author(s). Licensee IntechOpen. This chapter is distributed under the terms of the [Creative Commons Attribution-NonCommercial-ShareAlike-3.0 License](#), which permits use, distribution and reproduction for non-commercial purposes, provided the original is properly cited and derivative works building on this content are distributed under the same license.

IntechOpen

IntechOpen